UNCLASSIFIED

AD NUMBER

ADC000914

NEW LIMITATION CHANGE

TO

Approved for public release, distribution unlimited

FROM

Distribution limited to U.S. gov't. agencies only; Test and Evaluation; Jan 75. Other requests for this document must be referred to Director, Naval Research Lab., Washington, D. C. 20375.

AUTHORITY

NRL ltr., 5300-24, 11 Jun 1998

THIS PAGE IS UNCLASSIFIED

UNCLASSIFIED

AD NUMBER

C000 914

CLASSIFICATION CHANGES

TO

UNCLASSIFIED

FROM

CONFIDENTIAL

AUTHORITY

31 DEC 89 IAW OCA MARKINGS ON DOC

THIS PAGE IS UNCLASSIFIED

ADC000914

CONFIDENTIAL

NRL Report 7848

Shipboard Air Surveillance Radar Concepts: SENRAD I

[Unclassified Title]

S. K. MEADS

Search Radar Branch
Radar Division

January 17, 1975

"NATIONAL SECURITY INFORMATION"

"Unauthorized Disclosure Subject to Criminal Sanctions"

DDC
RECEIVED
FEB 24 1975
D

NAVAL RESEARCH LABORATORY
Washington, D.C.

CONFIDENTIAL

CONFIDENTIAL, classified by DIRNRL.
Exempt from GDS of E.O. 11652 by DIRNRL.
Ex. Cat. (3). Auto. declass. on Dec. 31, 1989.

Distribution limited to U.S. Government Agencies only; test and evaluation; January 1975. Other requests for this document must be referred to the Director, Naval Research Laboratory, Washington, D.C. 20375.

NATIONAL SECURITY INFORMATION

Unauthorized Disclosure Subject to Criminal Sanctions.

PREVIOUS REPORTS IN THIS SERIES

"SENRAD: An Advanced Search Radar Concept," R. D. Tompkins, editor, NRL Report 7713 (Secret Report, Unclassified Title), May 22, 1974.

CONFIDENTIAL

(This page is unclassified)

UNCLASSIFIED

SECURITY CLASSIFICATION OF THIS PAGE *(When Data Entered)*

REPORT DOCUMENTATION PAGE		READ INSTRUCTIONS BEFORE COMPLETING FORM
1. REPORT NUMBER NRL Report 7848	2. GOVT ACCESSION NO.	3. RECIPIENT'S CATALOG NUMBER
4. TITLE *(and Subtitle)* SHIPBOARD AIR SURVEILLANCE RADAR CONCEPTS: SENRAD I [Unclassified Title]		5. TYPE OF REPORT & PERIOD COVERED An interim report on an NRL continuing problem. 6. PERFORMING ORG. REPORT NUMBER
7. AUTHOR(s) S.K. Meads		8. CONTRACT OR GRANT NUMBER(s)
9. PERFORMING ORGANIZATION NAME AND ADDRESS Naval Research Laboratory Washington, D.C. 20375		10. PROGRAM ELEMENT, PROJECT, TASK AREA & WORK UNIT NUMBERS NRL Problem R02-86 RF 12-151-403-4152
11. CONTROLLING OFFICE NAME AND ADDRESS Department of the Navy Office of Naval Research Arlington, Va. 22217		12. REPORT DATE January 17, 1975 13. NUMBER OF PAGES 51
14. MONITORING AGENCY NAME & ADDRESS*(if different from Controlling Office)*		15. SECURITY CLASS. *(of this report)* Confidential 15a. DECLASSIFICATION/DOWNGRADING SCHEDULE XGDS-3 (1989)

16. DISTRIBUTION STATEMENT *(of this Report)*

Distribution limited to U.S. Government Agencies only; test and evaluation; January 1975. Other requests for this document must be referred to the Director, Naval Research Laboratory, Washington, D.C. 20375.

17. DISTRIBUTION STATEMENT *(of the abstract entered in Block 20, if different from Report)*

[redacted]

18. SUPPLEMENTARY NOTES

DDC RECEIVED FEB 24 1975 D

19. KEY WORDS *(Continue on reverse side if necessary and identify by block number)*

Air surveillance
Frequency agility
Shipboard radar
Wideband radar

20. ABSTRACT *(Continue on reverse side if necessary and identify by block number)*

(U) Concepts for a class of shipboard air surveillance radars capable of pulse-to-pulse agility in a 50% frequency band are described. Both two-dimensional (azimuth, range) and three-dimensional (azimuth, range, elevation) systems are described; however, the major emphasis is on the two-dimensional concept.

(U) The advantages of frequency-agile operation over a wide band are discussed. These are improved detection range in a noise jamming environment, reduction of the adverse effects

(Continued)

DD FORM 1 JAN 73 1473 EDITION OF 1 NOV 65 IS OBSOLETE S/N 0102-014-6601

UNCLASSIFIED

SECURITY CLASSIFICATION OF THIS PAGE *(When Data Entered)*

CONFIDENTIAL

(This page is unclassified)

20. Continued.

of interference pattern nulls, and elimination of MTI blind speeds.

(U) The calculated performance of the 2-D radar in a clear environment and in various clutter environments is discussed.

PREFACE

(C) This is the second report issued by the Radar Division of the Naval Research Laboratory (NRL) describing concepts for air surveillance radar systems having wideband frequency agility. Pulse-to-pulse frequency agility in two radar bands covering a 50% bandwidth is the basic feature of the SENRAD project, on which work has been under way at NRL for approximately two years.

(C) The first SENRAD report, NRL Report 7713, describes a stacked-beam radar capable of coarse height determination. The waveforms described for that radar feature pulses segmented into four subpulses, each at a different frequency. The combination of stacked beams and four-frequency waveforms led to a requirement for a large number of receiver-processor channels, and this, in turn, impacted unfavorably on estimated costs of the system.

(U) An assessment of the probable cost of the stacked-beam radar led to the evolution of the concepts for simpler two- and three-dimensional radars presented in this report.

CONTENTS

SHIPBOARD AIR SURVEILLANCE RADAR CONCEPTS: SENRAD I
[Unclassified Title]

INTRODUCTION

(U) In the performance of Navy shipboard air surveillance radars, a number of areas can be identified in which major improvements are needed and can be achieved. Areas needing improvement include electronic counter-countermeasures (ECCM), moving target indication (MTI), and data rate. All of these characteristics impact on the capability of a radar to provide automatic detection and automatic tracking of multiple targets.

(C) Current air surveillance radars, particularly the two-dimensional (2-D) systems, are ineffective in a noise jamming environment. The reasons for this ineffectiveness are

1. These radars are constrained to operate in relatively narrow frequency bands.

2. They do not have pulse-to-pulse frequency agility.

3. Wide azimuth beamwidths (and low antenna gains) result from the combination of the low frequencies of operation and aperture limitations.

The fact that the radars operate in narrow frequency bands without frequency agility allows a noise jammer to concentrate his energy in a narrow spectrum and thus easily overpower the radar. The wide azimuth beamwidth permits a jammer to screen targets over a relatively wide azimuth angular sector without having to overcome the pattern disadvantage of radiating into the radar antenna sidelobes. For these reasons, it is apparent that major improvements can be made in the performance of 2-D air search radars in an electronic countermeasures (ECM) environment by utilizing a higher radio frequency so that narrower azimuth beamwidths can be achieved, and by designing the radars to operate with pulse-to-pulse frequency agility over the widest band possible.

(C) Several problems remain unsolved in the implementation of MTI systems for long-range air surveillance radars. One of these is the need to suppress returns from weather, or chaff, or both at ranges over 100 n.mi. without using a high pulse repetition frequency (PRF) with its attendant range ambiguities. An aspect of this problem is the "blind velocities" which occur at close spacing in the velocity spectrum if a PRF that gives unambiguous range values is used. This close spacing and the large widths which these MTI nulls must have to suppress the wide spectral returns from weather and chaff result in very little of the velocity spectrum being available for the detection of targets of interest. It will be shown later that frequency agility over a wide band can alleviate the problem of blind speeds.

Note: Manuscript submitted November 22, 1974.

(U) Another aspect of the MTI problem occurs when land clutter and weather clutter exist at the same range. Because of the different mean radial velocities typically associated with these two types of clutter (land is stationary, but rain may be blown by wind), it is impractical to use a single-notch velocity filter to suppress both. The notch width would have to be so great that many targets of interest would be suppressed.

(U) Automatic detection and tracking is, of course, achievable only if the MTI processing of a radar is sufficiently good to reduce false target reports to a manageable number. In an air surveillance radar there is, in general, a tradeoff between MTI performance and data rate. The slower the data rate, the more samples are available for processing and the more reliable are the target reports. Thus, for good clutter suppression, designers prefer a slower scan rate. On the other hand, to track maneuvering targets and to correlate target detections accurately with tracks in file, one needs to increase the antenna scan rate. The correlation problem is particularly difficult with high target densities and points to a need for a small resolution cell, as well as a high data rate. With improved MTI technology, the compromise data interval can be adjusted more toward the faster rates required for automatic tracking.

(U) Nulls are created at certain elevation angles in the radiation pattern of antennas overlooking a reflecting surface such as the sea. These nulls result from coherent addition of a direct ray and a ray reflected from the surface. The positions of the nulls are a function of the radiated frequency and the height of the antenna above the surface. Since the nulls result in an inability to detect targets at fixed altitudes throughout significant range sectors, they prevent reliable automatic tracking of targets at low elevation angles and long ranges. It is therefore desirable, if possible, to find a means to avoid loss of detection in the nulls. The null positions could be varied by varying the antenna height above the reflecting surface, but this is not a practical approach. The same effect can be achieved by varying the radiated frequency over a wide range, and this is more practical. Therefore, by transmitting several frequencies spaced over about a 50% bandwidth in each azimuth beamwidth, the effect of the interference nulls can be largely eliminated. That is, since the null positions move with frequency change, if a target is illuminated by several relatively widely spaced frequencies, it is likely that the target will be in a high field region for at least one of the frequencies.

(C) In this report, concepts are described for both 2-D and 3-D air surveillance radars, each applicable to different sets of ship classes. These concepts are aimed at achieving major improvements in the problem areas discussed above. The major feature of the radars is a capability for pulse-to-pulse frequency agility throughout both the 900- and 1300-MHz radar bands and throughout most of the frequency spectrum between these bands.

ADVANTAGES OF WIDE-BANDWIDTH OPERATION

(C) Three major benefits are derived from the capability to operate simultaneously in two widely separated bands, with pulse-to-pulse frequency agility in these bands. As indicated above, these benefits are (a) a noise jammer is forced to spread his radiated energy over a wide band, (b) interference nulls in the elevation coverage pattern are largely eliminated, and (c) MTI "blind speeds" are effectively eliminated. These improvements are now discussed in some detail.

Noise Jamming

(C) The equations for calculating detection ranges of a self-screening target and a target screened by a standoff jammer [1] are, respectively,

$$R_{SS} = 4.817 \times 10^{-3} F_t \left[\frac{P_t \tau G_t \sigma}{P_{tj} G_j V_0 C_B L} \right]^{1/2}$$

and

$$R_{SOJ} = 6.940 \times 10^{-2} \left[\frac{P_t \tau G_t \sigma F_t^2 F_r^2 R_j^2}{P_{tj} G_j F_j^2 V_0 C_B L} \right]^{1/4},$$

where

P_t = radar pulse power (kW)

τ = radar pulse length (μs)

G_t = transmitter antenna gain

F_t = transmitter pattern propagation factor

F_r = receiver pattern propagation factor

σ = target cross section

P_{tj} = power radiated by the jammer (W/MHz)

G_j = jammer antenna gain

F_j = jammer pattern propagation factor

V_0 = visibility factor (required S/N)

C_B = radar bandwidth correction factor

L = radar losses.

Assume that a number of air search radars are designed with identical characteristics with the exception of the bandwidth in which they are capable of pulse-to-pulse frequency agility. Assume also that a noise jammer is limited by weight considerations to a particular total radiated power and that the operator can concentrate that jamming power in

any band segment(s) of 10-MHz or greater width. Then, for purposes of comparison of the performance of the radars against the noise jammer, the equations above can be re-written as

$$R_{SS} = K_1 \, (P_{tj})^{-1/2}$$

and

$$R_{SOJ} = K_2 \, (P_{tj})^{-1/4}.$$

Generally speaking, an operator will find it necessary to spread the energy of his noise jammer over the total agility bandwidth of a radar, if that is possible, since it is not possible to anticipate the frequency on which the radar will transmit next. Thus, unless he can radiate enough power throughout the band to exceed the integrated skin returns, it is not possible for a jammer to deny range determination against the jammer-bearing vehicle or any target closer to the radar. The so-called "fast set-on" jammer can concentrate energy on the current-pulse radar frequency so as to deny range determination against targets at ranges greater than that of the jammer. This type of jammer can also deny range determination against targets at all ranges in an environment that requires the radar to perform doppler filtering, since the radar frequency must be maintained constant throughout the coherent integration period and the jammer can be set on that frequency within a few microseconds after being illuminated by the first pulse of a train.

(C) If the jammer must spread his energy over the agility bandwidth of the radar Δf then his effective radiated power P_{tj} is inversely proportional to Δf. Thus, the self-screening and standoff jammer range equations can be rewritten as

$$R_{ss} = K_1 \, (\Delta f)^{1/2}$$

and

$$R_{SOJ} = K_2 \, (\Delta f)^{1/4}.$$

These equations can be used to show that a radar operating with frequency agility over a 275-MHz band, against a self-screening jammer, will achieve a detection range 5.2 times that achieved by the same radar operating at a fixed frequency. Similarly, a range 2.3 times as great will be achieved against a target screened by a standoff jammer. In both cases, it is assumed that the jammer energy will be spread over a 10-MHz band against the fixed-frequency radar.

Elimination of Elevation Pattern Interference Nulls

(U) The phenomenon that occurs when a radar overlooks a reflecting surface such as the sea has been analyzed by many researchers. The free-space radiation patterns are modified by the presence of a wave reflected from the surface. The pattern in the vertical plane is the result of phasor-vector addition of the direct and reflected waves. In the maxima of

this interference pattern, radar echo signals may be increased by as much as 12 dB compared to the free-space signal, whereas in the minima, or nulls, the signal strength may theoretically go to zero. Blake [2] has developed computer programs for plotting the vertical-plane coverage diagram of a radar. These programs, with some modifications, were used to generate the diagrams that appear in this section.

(U) Figure 1 shows the vertical-plane coverage diagram for a radar operating at 900 MHz with the antenna at a height of 75 ft above the sea. The calculated free-space range of the radar is 148 n.mi. for detecting a 1-m^2 target. The vertical antenna pattern is 10° at the 3-dB points with cosecant-squared shaping to 30° above the horizon. The nose of the beam is tilted 3° above the horizon. The sea surface is assumed to be relatively smooth, with maximum wave heights of 1 ft.

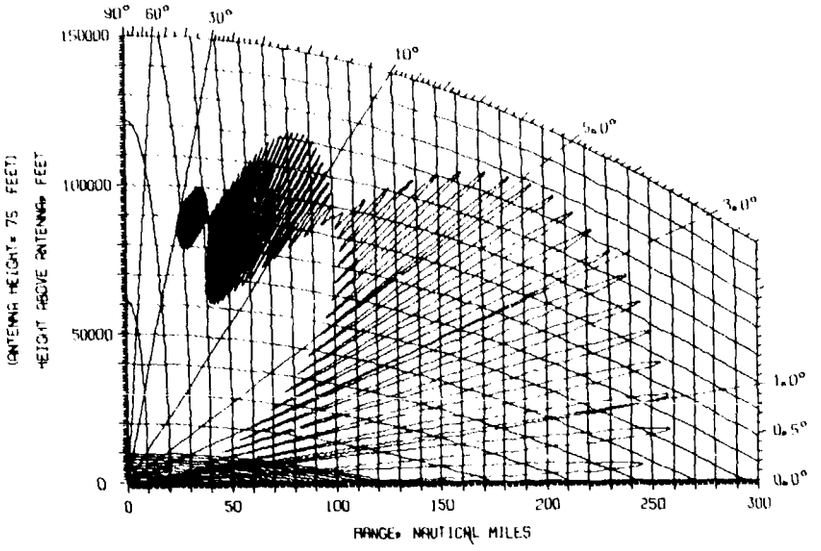

(U) Fig. 1 — Range-height coverage diagram for a single-freguency (900-MHz) radar

(U) Observation of Fig. 1 indicates that a 1-m^2 target flying a radial course toward the radar at an altitude of 40,000 ft will first be detected at a range of 230 n.mi. The target will remain detectable to the radar to a range of 222 n.mi., at which point it becomes undetectable and remains so until it reaches a range of 204 n.mi. Thus, over a range sector of 18 n.mi., the target is not detectable. As the target continues toward the ship, there are eight other range sectors in which detection is not achieved, the last one occurring at a range of 87 n.mi. Obviously, these gaps will cause difficulty in maintaining a track on the incoming target.

(C) If the target described above is illuminated with several pulses of widely spaced frequencies on each scan of the antenna, the range sectors in which detection is not achieved are largely eliminated. For example, Fig. 2 shows a composite vertical-plane coverage diagram in which the maximum range achieved with one of four frequencies (850, 940, 1215, and 1400 MHz) is plotted at each elevation angle. Antenna height and sea state are the same as indicated before. The vertical antenna pattern is again 10° at the 3-dB points for 850 and 940 MHz, but 7° for 1215 and 1400 MHz. For both bands, $\csc^2$ shaping to 30° elevation is assumed. Free-space ranges used in this calculation are 142 n.mi. for the 850-940 MHz band and 154 n.mi. for the 1215-1400 band. It might be noted that these free space ranges are achieved on each of four frequencies with twice the average power required to achieve the 148 n.mi. with a single frequency. The quantities affecting the range calculation that are varied for the two cases include the following:

1. Number of pulses integrated: Six for the single-frequency chart, 3 and 2 for the low and high bands, respectively, on the four-frequency chart. The latter numbers result from maintaining a constant data rate for the two cases and doubling the average power for the four-frequency case so that transmissions on the low and high bands can be made simultaneously.

2. Swerling target fluctuation case: A Case 1 fluctuation model, typical of aircraft targets, is assumed for the single-frequency calculation. A Case 2 (fast fluctuation) target model is assumed for the four-frequency calculation, since the frequency changes should cause a pulse-to-pulse fluctuation of the target return.

In Fig. 2 it may be observed that a target flying a radial inbound course at an altitude of 40,000 ft is rarely lost after initial detection, and then only in very small range sectors.

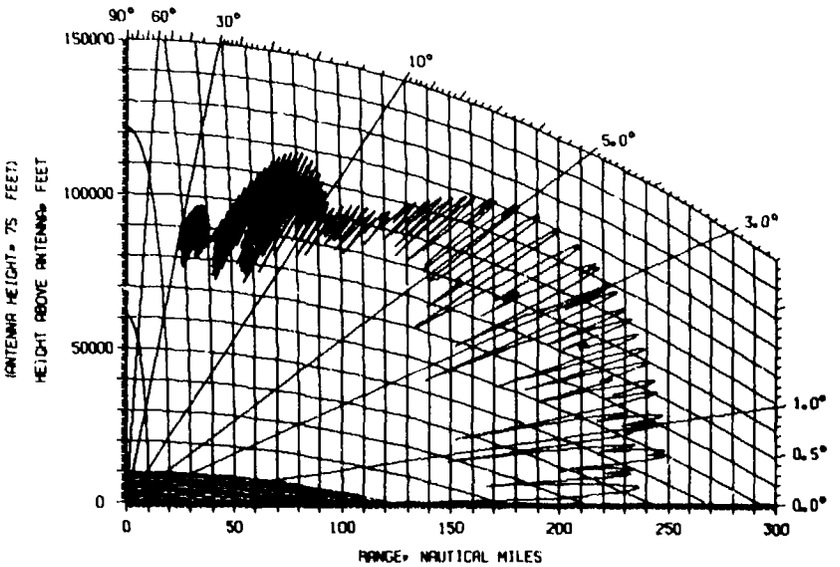

(C) Fig. 2 — Range-height coverage diagram showing maximum response from one of four frequencies (850, 940, 1215, 1400 MHz) at each elevation angle

(U) Another method of presenting the effect of the interference of direct and reflected rays, which is more easily interpreted, is illustrated in Figs. 3 and 4. These charts show signal level vs range for a target at a specific altitude. The signal level is normalized so that the 0-dB level represents the minimum detectable signal. Figure 3 shows the signal level obtained by a single-frequency radar (900 MHz), on a 1-m^2 target at 10,000 ft altitude. This diagram and the one which follows are for a low-insensitivity mode of the radar (e.g., MTI mode), with a free-space range of 58 n.mi. The range sectors in which detection is not possible are quite obvious here.

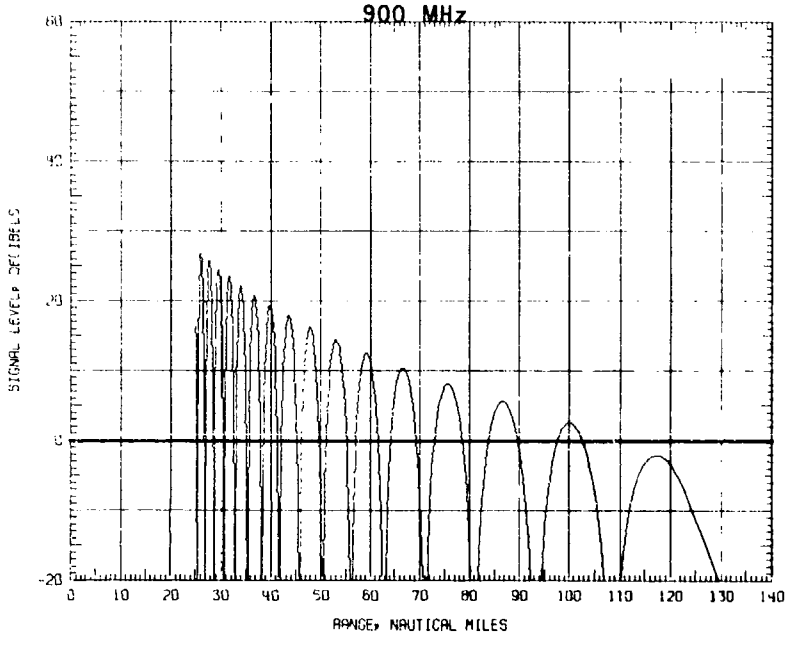

(U) Fig. 3 — Signal level vs range for a single-frequency (900-MHz) radar on a target at 10,000 ft altitude

(C) Figure 4 shows signal level vs range for four frequencies plotted on a single graph. At ranges less than 100 n.mi., the range sectors in which detection on at least one of the four frequencies is not possible are few in number and of very limited extent.

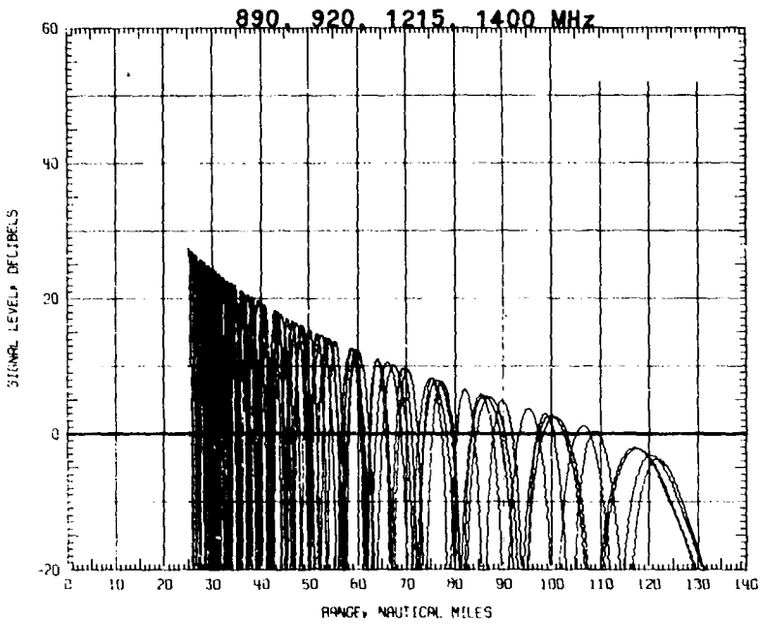

(C) Fig. 4 — Composite graph of signal level vs range for four transmitted frequencies (890, 920, 1215, 1400 MHz) on a target at 10,000 ft altitude

Elimination of MTI Blind Speeds

(U) A similarly dramatic improvement can be made in the elimination of MTI "blind speeds". If a target is moving with respect to the radar at a radial velocity such that the doppler shift in the return from the target is a multiple of the radar PRF, the target return will be suppressed in an MTI processor. This phenomenon is illustrated in Fig. 5, which shows the MTI response vs velocity for a 3-pulse canceler on a 900-MHz radar with a 1000 pulse repetition frequency. Blind speeds occur at multiples of about 310 knots. This difficulty may be alleviated by using a staggered-interval pulse train with a digital MTI canceler, but in order to fill in the nulls in the response curve, a large percentage variation in the PRF is required. That leads to inefficient use of radar time, since the minimum pulse interval must correspond to the desired instrumented range of the MTI [3]. Further, even with an optimized design [4], the variations in MTI response vs velocity are as great as 26 dB.

(C) The use of agility in the radio frequency radiated, if possible over a wide band, allows one to eliminate MTI blind speeds without inefficient use of radar time and with minimal variations of filter response vs frequency. Figure 6 shows a composite curve in which the maximum response achieved at any one of four frequencies for a given target velocity is plotted. This curve again is calculated for a 3-pulse canceler, with a constant PRF of 1000. It is assumed that during a scan of the antenna each target is illuminated with at least four 3-pulse trains and that each train is at a different radio frequency. As may be

seen, the maximum variation of the response curve is approximately 12 dB; the first true blind speed, which is not shown in the illustration occurs at a velocity of ~60,000 knots, well above the range of velocities of targets of interest.

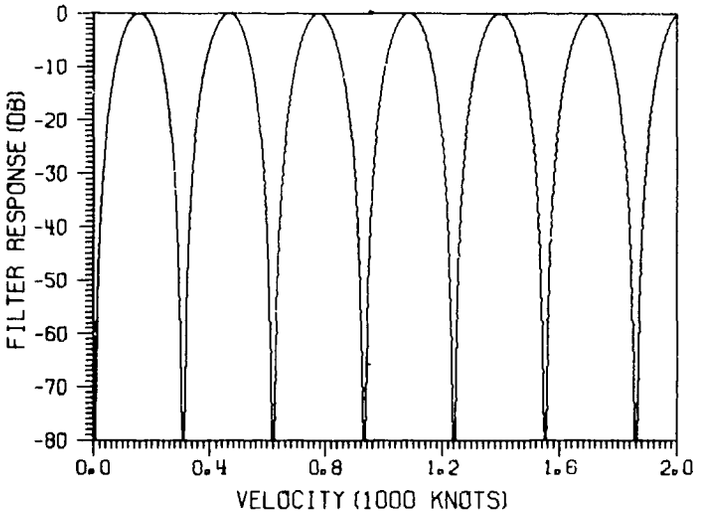

(U) Fig. 5 — MTI velocity response curve for a 3-pulse canceler on a single-frequency (900-MHz) radar with PRF of 1000 pps.

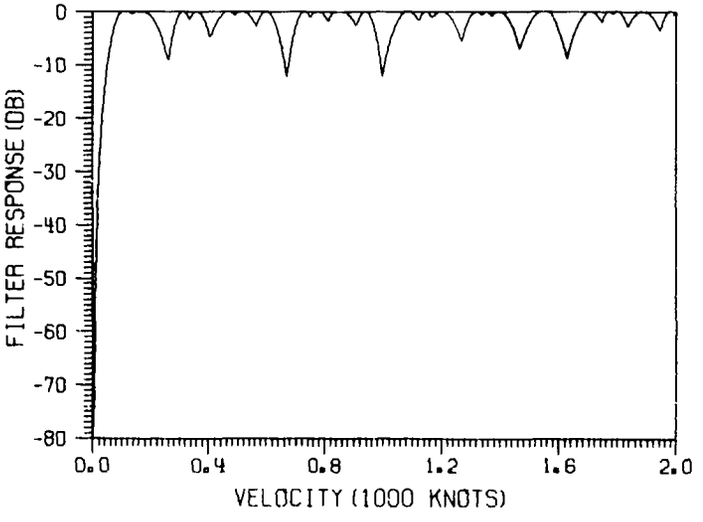

(C) Fig. 6 — MTI velocity response curve of a 3-pulse canceler showing maximum response achieved at one of four frequencies for each velocity. Pulse repetition frequency is 1000 pps.

(C) It has been shown that the capability of operating in a wide range of frequencies, with frequency band end points at approximately ±25% of the center frequency, leads to major performance improvements in ECCM, elimination of nulls in the elevation coverage, and elimination of MTI blind speeds It should be pointed out that there may be combinations of noise jamming environment, target elevation angle, and target velocity that prevent obtaining a strong return on any one frequency within even a 50% bandwidth. However, the probability of not obtaining a strong return on one frequency of the wideband radar is small compared to the probability in the case of the narrowband radar.

DESCRIPTION OF TWO-DIMENSIONAL RADAR

(C) In this section a concept for a 2-D air search radar intended for shipboard installation is discussed. Some of the major features of the proposed radar are listed below.

Frequency	850-942 and 1215-1400 MHz (capable of operation at frequencies of 850-1050 and 1100-1400 MHz)
Antenna	Array, stabliized for roll and pitch
Data rate	4 s
Modes	(1) Long-range search combined with land and sea clutter MTI (2) Antichaff/weather MTI

(C) High-quality MTI processing will reduce false alarms to a level that permits reliable automatic detection. This characteristic, together with a 4-s data rate and a relatively small resolution cell, will permit automatic tracking (track-while-scan) of multiple targets.

(C) A basic block diagram of the radar system is shown in Fig. 7. Essentially, two separate transmitter-receivers, one operating in the 900-MHz band and one in the 1300-MHz band, are diplexed into a single antenna. Transmissions on the two bands occur simultaneously. Received signals, after pulse compression, MTI processing, and CFAR (constant false alarm rate) processing in the individual channels, are combined for detection, beam splitting, automatic track extraction, and display. A control computer performs the function of frequency selection, based on a clear-channel search, programmed sequence, or pseudorandom selection. The computer also translates ship's motion information from the stable element to stabilization commands for the antenna pedestal.

(U) More detailed descriptions of several of the major components of the radar are provided in the following sections.

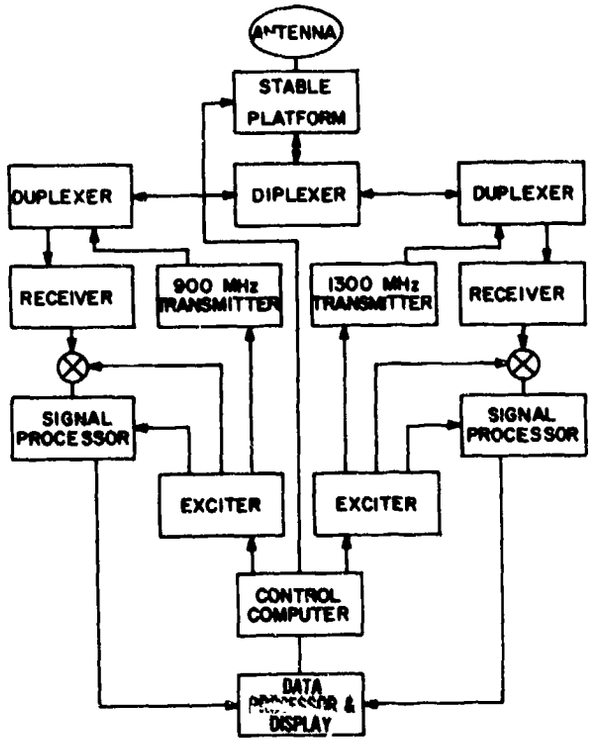

(C) Fig. 7 — Two-dimensional radar system

Antenna

(C) The preferred antenna approach is to use an array of printed dipoles, as shown in Fig. 8. The array is approximately 8 ft high by 20 ft wide and consists of 16 rows of 32 dipoles each. A printed-circuit corporate feed board feeds each row of dipoles. A single high-power vertical feed distributes the transmitted power among the 16 rows. To reduce wind loading, the spaces between the horizontal feed boards are kept open insofar as possible.

(C) The pedestal provides azimuth drive over roll and pitch stabilization. This is a departure from current 2-D shipboard air search radars, which are generally unstabilized and at the most have line-of-sight stabilization. Roll and pitch stabilization, together with the relatively narrow beamwidth of this antenna, will permit measurements of azimuth positions of targets with a standard deviation no greater than 0.5°. An analysis by Cantrell and Trunk [5] shows that with this order of accuracy the probability that a weapon control radar can acquire a target directly from the 2-D search radar is quite high. Thus, the need for an intermediate 3-D radar is eliminated.

(U) To minimize the weight of the antenna, a carbon-epoxy composite material developed for satellite applications will be used to the maximum extent possible, both for support

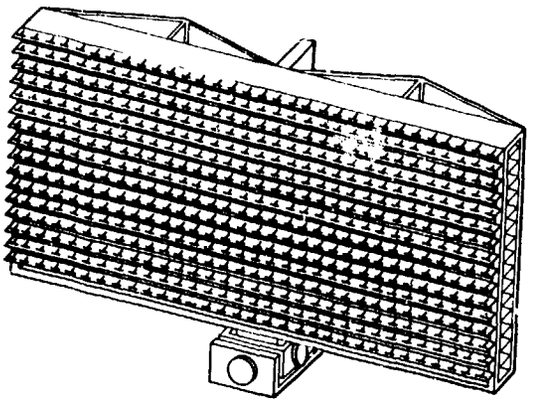

(U) Fig. 8 — Array antenna for 2-D radar

structure and for feeds and radiators. It is estimated that with this material the total masthead weight of the antenna and pedestal can be kept below 2,000 lb.

(C) A wideband printed-dipole radiator has been developed at NRL [6]. This radiator was tested in a number of configurations of waveguide array simulators. Over the 850-1440 MHz band, it exhibits a VSWR of less than 2.8:1.

(C) Some calculated characteristics of the antenna are listed below.

Array size	8 ft high by 20 ft wide
Number of dipoles	512
Azimuth beamwidth	
850 MHz	3.5°
1400 MHz	2.4°
Elevation beamwidth	
850 MHz	10°, $\csc^2$ to 30°
1400 MHz	7°, $\csc^2$ to 30°
Gain	
850 MHz	29 dB
1400 MHz	32 dB
Peak azimuth sidelobes	-25 dB
Polarization	Horizontal
Weight (including pedestal)	< 2000 lb

(U) Although the antenna described here is an array of dipoles, investigation of a parabolic-reflector approach, which might have weight advantages, is continuing. The array approach is preferred because of the better control of aperture illumination it provides, thereby permitting the attainment of lower sidelobes, an important ECCM feature.

Transmitter

(C) Each of the two transmitters in the baseline system design has a wideband, ring-bar traveling wave tube (TWT) as a final amplifier. Raytheon's type QKW1722 tube operates in the 1300-MHz band. Typical operating characteristics [7] for this tube are as follows.

Peak power	160 kW
Duty cycle	0.0625
Maximum pulse length	2000 μs
Average power	10 kW
1-dB bandwidth	1100-1400 MHz
Power gain	50 dB

This tube is grid-pulsed, liquid-cooled, and is identical to the QKW1518SG, except that it uses an integral solenoid for focusing. Because of the high gain of this tube, the driver chain may consist only of transistor amplifiers.

(C) No suitable tube currently exists for the 900-MHz band. It will therefore be necessary to develop a model of the QKW1722 scaled for that band. Compared to other tube developments, this should entail comparatively little risk.

(C) An alternative transmitter approach would use a single TWT to cover the entire 850- to 1400-MHz band. Such a tube is currently under development in the Electronics Division of the Naval Research Laboratory. Performance goals for this tube, which is a helix type with liquid cooling of the helix, are listed below.

Peak power	300 kW
Duty cycle	0.05
Maximum pulse length	250 μs
Average power	15 kW
1-dB Bandwidth	850-1400 MHz
Power gain	25 dB

If this tube is successfully developed, it will be used in a single transmitter to replace the two transmitters shown in Fig. 7. Two receive channels would still be required. Development of this tube is considered a project of significantly higher risk than the scaling of the QKW1722.

Modes of Operation

(C) Two operating modes are available for this radar, with mode selection an operator option. Mode 1 is the clear-sky search mode, in which an MTI pulse burst which is effective against area clutter is interspersed with pulses used for long-range search. Mode 2 is designed for a volume clutter (rain, chaff) environment and utilizes an MTI implemented over the full range sweep. Since both modes use the same antenna scan rate, either may be selected under computer control on an azimuth sector basis. For example, if rain or chaff exists in a certain azimuth sector, Mode 2 operation may be designated for that sector while Mode 1 operation is used for all other azimuth sectors.

Clear-Sky Mode (Mode 1)

(C) In this mode, a 3-pulse MTI group is interspersed with long-range search pulses. Separation of the pulses in the MTI group is 1 ms, and MTI is implemented to a range of 80 n.mi. For the long-range pulses, a range sweep of 3.1 ms is provided, permitting range measurements up to 250 n.mi.

(C) Simultaneous transmissions are made in the 900- and 1300-MHz bands. The clear-sky waveform for one frequency band is shown in Fig. 9. At a 4-s data rate, approximately 26.7 ms are available during the rotation of the antenna through one 3-dB azimuth beamwidth at 1400 MHz, and 38.9 ms are available per 3-dB beamwidth at 850 MHz. Thus, the complete sequence of pulses shown in Fig. 9 will illuminate a target within a 3-dB beamwidth at the highest frequency, and half again as many pulses will be transmitted within the 3-dB beamwidth at the lowest frequency range.

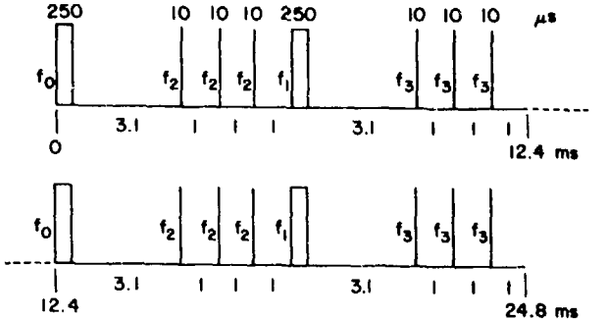

(C) Fig. 9 — Clear-sky (Mode 1) waveform showing pulses from one transmitter during antenna rotation through one azimuth beamwidth (24.8 ms).

(C) It may be seen in Fig. 9 that the transmitted frequency is changed from pulse to pulse except within the MTI groups and is changed from one MTI group to the next. Although the illustration shows the long-range pulses and the MTI groups oscillating between two values, it is not necessary to do this; i.e., there is no necessity to repeat frequencies in any particular order. When the sequence shown in Fig. 9 is used, the second transmitter is transmitting another group of pulses in a different frequency band in synchronism with the pulse sequence shown. On each antenna scan, a target will be illuminated with high-energy pulses at four different frequencies and with MTI pulse groups at four different frequencies. This represents the minimum frequency change for this mode. If frequencies are not repeated, however, the total frequencies become 10 and 10 (4 and 4 in the high band plus 6 and 6 in the low band due to the wider antenna beamwidth at the low band).

(C) Range calculation worksheets [1] for the MTI waveform and the long-range waveform are shown in Figs. 10 and 11, respectively. A worst-case number of pulses for noncoherent integration is assumed (eight for each calculation). The MTI processor is a 3-pulse canceler, and hence only one output is generated for each 3-pulse group. Swerling Case 2 target fluctuation characteristics are assumed for both MTI and non-MTI processing. This assumption can be made because of the pulse-to-pulse and group-to-group frequency agility of the radar. The pattern propagation factor is taken to be 1.56, since that is the average value obtained against relatively low-elevation targets, when the averaging is done across an elevation sector containing one or more interference lobes. A midband frequency is used for the range calculations, which are for 0.5 probability of detection and 10^{-8} probability of false alarm. Miscellaneous losses L_x listed on the calculations include 2.2 dB for pulse compression and 1.5 dB for MTI processing. The calculated ranges (item 11) are 92 n.mi. for the MTI waveform and 215 n.mi. for the long-range waveform.

Rain and Chaff Mode (Mode 2)

(C) In this mode a sequence of pulses is transmitted with an interpulse spacing appropriate for an unambiguous range of 80-n.mi. After 14 pulses at one frequency, the radio frequency is shifted and the PRF is shifted slightly. This mode is instrumented to 160 n.mi., and hence, a range ambiguity exists in the output data. The purpose of the shift in PRF is to remove that ambiguity.

(C) As in Mode 1, simultaneous transmissions are made in the 900- and 1300-MHz bands. A pulse length of 60 μs is used to obtain sufficient sensitivity at the maximum range of 160 n.mi. The sequence of 14 pulses requires 14.7 ms, so that two such sequences will be transmitted within the 3-dB azimuth beamwidth at all but the highest frequencies.

(C) Velocity filtering for this mode is a three-stage process. The first stage is a 3-pulse canceler with its velocity notch centered on the velocity of the surface clutter (sea and land). The second stage is again a 3-pulse canceler, but with its velocity notch centered on the mean velocity of the volume clutter. The third stage is an 8-point fast Fourier transform (FFT) velocity filter bank. Range extent gates are used in conjunction with the FFT to eliminate either land, rain, or chaff residues that are extended in range. Finally, a low-velocity blanker loop is closed around the 3-stage velocity filter to remove those fixed clutter residues which are not sufficiently extended in range to be removed

PULSE-RADAR RANGE-CALCULATION WORK SHEET

For use in conjunction with NRL Report 6930 (Dec. 1969). Based on Eq. (13), page 10, and associated auxiliary equations and curves as referenced below.

1. Compute the system input noise temperature T_s, following the outline in section A below.
2. Enter range factors known in other than decibel form in section B below, for reference.
3. Enter logarithmic and decibel values in section C below, positive values in the plus column and negative values in the minus column. For example, if $V_{0\,(dB)}$ as given by Figs. 4 through 9 is negative, then $-V_{0\,(dB)}$ is positive and goes in the plus column. For C_B, see Figs. 1 through 3. For definitions of the range factors, see Eq. (13).

Radar antenna height: h = ft. Target elevation angle: θ = 0.5 °. (See Fig. 13.)

A. Computation of T_s:

$T_s = T_a + T_r + L_r T_e$

(a) Compute T_a.
For $T_{tg} = T_{ta} = 290$ and $T_d = 36$ use Eq. (37a).
Read T_a' from Fig. 11.
$L_{a(dB)}$: 2.0 L_a: 1.585
$T_a = (0.876\,T_a' - 254)/L_a + 290$
T_a = 234 °K

(b) Compute T_r using Eq. (40).
For T_{tr} = 290 use Table 1.
$L_{r(dB)}$: 2.5 T_r = 226 °K

(c) Compute T_e using Eq. (41) or using Table 1.
$F_{n(dB)}$: 4 T_e: 438 °K
L_r: 1.778 $L_r T_e$ = 779°K

Add. T_s = 1239°K

B. Range Factors		C. Decibel Values	Plus (+)	Minus (-)
$P_{t\,(kW)}$	160	10 log $P_{t\,(kW)}$	22.0	.
$\tau_{\mu sec}$	10	10 log $\tau_{\mu sec}$	10.0	.
G_t	1122	$G_{t\,(dB)}$	30.5	.
G_r	1122	$G_{r\,(dB)}$	30.5	.
$\sigma_{(sq\,m)}$	1	10 log σ	.	.
f_{MHz}	1125	-20 log f_{MHz}	.	61.0
T_s (°K)	1239	-10 log T_s	.	30.9
V_0	8 pulses	$-V_{0\,(dB)}$	.	5.7
C_B	—	$-C_{B\,(dB)}$		—
L_t	2.0 dB	$-L_{t\,(dB)}$		2.0
L_p	1.6 dB	$-L_{p\,(dB)}$		1.6
L_x	2.2 + 1.5	$-L_{x\,(dB)}$		3.7
Range-equation constant (40 log 1.292)			4.45	
4. Obtain the column totals →			97.5	104.9
5. Enter the smaller total below the larger →			.	97.5
6. Subtract to obtain the net decibels (dB) →			+ ,	-7.4

7. In Table 2 find the range ratio corresponding to this net decibel (dB) value, taking its sign (±) into account. Multiply this ratio by 100. This is R_0 → 65.3
8. Multiply R_0 by the pattern-propagation factor F = 1.56 (see Eqs. (42) through (65) and Figs. 12 through 19): $R_0 \times F = R'$ → 102
9. On the appropriate curve of Figs. 21 and 22 determine the atmospheric-absorption loss factor, $L_{a(dB)}$, corresponding to R'. This is $L_{a(dB)(1)}$. → 1.75 dB
10. Find the range factor δ_1 corresponding to $-L_{a(dB)(1)}$ from the formula δ = antilog $(-L_{a(dB)}/40)$ or by using Table 2. → 0.9042
11. Multiply R' by δ_1. This is a first approximation of the range R_1. → 92
12. If R_1 differs appreciably from R', on the appropriate curve of Figs. 21 and 22, find the new value of $L_{a(dB)}$ corresponding to R_1. This is $L_{a(dB)(2)}$. →
13. Find the range-increase factor (Table 2) corresponding to the difference between $L_{a(dB)(1)}$ and $L_{a(dB)(2)}$. This is δ_2. →
14. Multiply R_1 by δ_2. This is the radar range in nautical miles, R. →

Note: If the difference between $L_{a(dB)(1)}$ and $L_{a(dB)(2)}$ is less than 0.1 dB, R_1 may be taken as the final range value, and steps 12 through 14 may be omitted. If $L_{a(dB)(1)}$ is less than 0.1 dB, R' may be taken as the final range value, and steps 9 through 14 may be omitted. (For radar frequencies up to 10,000 megahertz, correction of the atmospheric attenuation beyond the $L_{a(dB)(2)}$ value would amount to less than 0.1 dB.)

(C) Fig. 10 — Detection range-calculation worksheet completed for Mode 1 MTI waveform; 0.5 P_d, 10^{-8} P_{fa} on a 1-m^2 target

PULSE-RADAR RANGE-CALCULATION WORK SHEET

For use in conjunction with NRL Report 6930 (Dec. 1969). Based on Eq. (13), page 10, and associated auxiliary equations and curves as referenced below.

1. Compute the system input noise temperature T_s, following the outline in section A below.
2. Enter range factors known in other than decibel form in section B below, for reference.
3. Enter logarithmic and decibel values in section C below, positive values in the plus column and negative values in the minus column. For example, if $V_{0\,(dB)}$ as given by Figs. 4 through 9 is negative, then $-V_{0\,(dB)}$ is positive and goes in the plus column. For C_B, see Figs. 1 through 3. For definitions of the range factors, see Eq. (13).

Radar antenna height: h = ft. Target elevation angle: θ = 0.5°. (See Fig. 13.)

A. Computation of T_s:

$T_s = T_a + T_r + L_r T_e$

(a) Compute T_a.
For $T_{tg} = T_{ts} = 290$ and $T_g = 36$ use Eq. (37a).
Read T_a' from Fig. 11.
$L_{a\,(dB)}$: 2.0 L_a: 1.585
$T_a = (0.876\,T_a' - 254)/L_a + 290$
T_a = 334 °K

(b) Compute T_r using Eq. (40).
For $T_{tr} = 290$ use Table 1.
$L_{r\,(dB)}$: 2.5 T_r = 226 °K

(c) Compute T_e using Eq. (41) or using Table 1.
$F_{n\,(dB)}$: 4 T_e: 436 °K
L_r: 1.778 $L_r T_e$ = 779°K

Add. T_s = 1239 °K

B. Range Factors		C. Decibel Values	Plus (+)	Minus (−)
$P_{t\,(kW)}$	160	10 log $P_{t\,(kW)}$	22·0	·
$\tau_{\mu sec}$	250	10 log $\tau_{\mu sec}$	24·0	·
G_t	1122	$G_{t\,(dB)}$	30·5	·
G_r	1122	$G_{r\,(dB)}$	30·5	·
$\sigma_{(sq\ m)}$	1	10 log σ	·	·
f_{MHz}	1125	−20 log f_{MHz}	·	61·0
T_s (°K)	1239	−10 log T_s	·	30·9
V_0	8 pulses	$-V_{0\,(dB)}$	·	5·7
C_B	—	$-C_{B\,(dB)}$		—
L_t	2.0 dB	$-L_{t\,(dB)}$		2·0
L_p	1.6 dB	$-L_{p\,(dB)}$		1·6
L_x	2.2 dB	$-L_{x\,(dB)}$		2·2
Range-equation constant (40 log 1.292)			4.45	
4. Obtain the column totals →			111·5	103·4
5. Enter the smaller total below the larger →			103·4	·
6. Subtract to obtain the net decibels (dB) →			+8.1	− ·

7. In Table 2 find the range ratio corresponding to this net decibel (dB) value, taking its sign (±) into account. Multiply this ratio by 100. This is R_c → 159
8. Multiply R_0 by the pattern-propagation factor [F = 1. / $R_0 \times F$ =] (see Eqs. (42) through (65) and Figs. 12 through 19): → 248
9. On the appropriate curve of Figs. 21 and 22 determine the atmospheric-absorption loss factor, $L_{a\,(dB)}$, corresponding to R'. This is $L_{a\,(dB)(1)}$. → 2.5
10. Find the range factor δ_1 corresponding to $-L_{a\,(dB)(1)}$ from the formula δ = antilog $(-L_{a\,(dB)}/40)$ or by using Table 2. → 0.866
11. Multiply R' by δ_1. This is a first approximation of the range R_1. → 215
12. If R_1 differs appreciably from R', on the appropriate curve of Figs. 21 and 22, find the new value of $L_{a\,(dB)}$ corresponding to R_1. This is $L_{a\,(dB)(2)}$. →
13. Find the range-increase factor (Table 2) corresponding to the difference between $L_{a\,(dB)(1)}$ and $L_{a\,(dB)(2)}$. This is δ_2. →
14. Multiply R_1 by δ_2. This is the radar range in nautical miles, R. →

Note: If the difference between $L_{a\,(dB)(1)}$ and $L_{a\,(dB)(2)}$ is less than 0.1 dB, R_1 may be taken as the final range value, and steps 12 through 14 may be omitted. If $L_{a\,(dB)(1)}$ is less than 0.1 dB, R' may be taken as the final range value, and steps 9 through 14 may be omitted. (For radar frequencies up to 10,000 megahertz, correction of the atmospheric attenuation beyond the $L_{a\,(dB)(2)}$ value would amount to less than 0.1 dB.)

(C) Fig. 11 — Detection range calculation worksheet completed for Mode 1 long-range waveform; 0.5 P_d, 10^{-8} P_{fa} on a 1-m^2 target

by the range-extent gates and which are of sufficiently large amplitude to exceed the cancellation ratio of the first 3-pulse canceler.

(C) The rain/chaff mode waveform for one frequency band is shown in Fig. 12. The same pulse groups are transmitted simultansously on the second frequency band. Therefore, as in Mode 1, each target will be illuminated by at least four frequencies within the 3-dB antenna beamwidth.

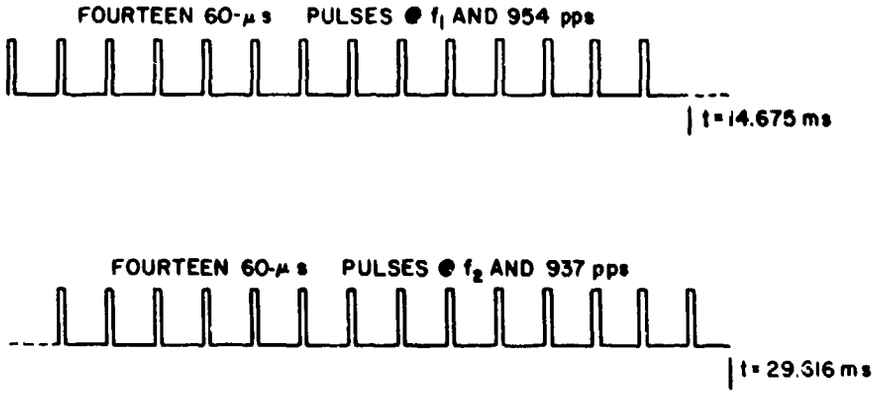

(C) Fig. 12 — Rain/chaff (Mode 2) waveform showing pulses from one transmitter during antenna rotation through one azimuth beamwidth (29.616 ms).

(C) A range calculation worksheet for the rain/chaff mode is shown in Fig. 13. Only one report emanates from the MTI system for each sequence of 14 pulses received. Thus, since there are two sequences on each band, four outputs from the MTI are available for noncoherent integration. For the reasons discussed in the previous section, the target is again considered to exhibit the Swerling Case 2 fluctuation characteristics, and the pattern propagation factor is taken as 1.56. Miscellaneous losses listed for this mode include 2.2 dB for pulse compression and 3 dB for MTI processing. These losses are more than offset by a 9-dB coherent integration gain for the 8-point FFT velocity filter. The calculated range is 183 n.mi. It should be noted that in this mode somewhat poorer azimuth beam-splitting performance results, since only two reports per target are obtained.

Signal Processing

(C) The signal processing approach is shown conceptually in Figs. 14, 15, and 16. Received signals are separated into the two bands by the diplexer (Fig. 7), and each signal passes through an individual duplexer and into an RF preamplifier. As shown in Fig. 14, after IF amplification and signal processing, the signals from the two bands are added prior to video integration, detection, and data processing. The signal channels shown in the center of Fig. 14, consisting only of IF amplifiers and pulse compressors, process the long-range pulses for Mode 1 operation. The pulse-compression networks have a compression ratio of 500:1, so that the 250-μs transmitted pulses are compressed to 0.5 μs.

PULSE-RADAR RANGE-CALCULATION WORK SHEET

For use in conjunction with NRL Report 6930 (Dec. 1969). Based on Eq. (13), page 10, and associated auxiliary equations and curves as referenced below.

1. Compute the system input noise temperature T_s, following the outline in section A below.
2. Enter range factors known in other than decibel form in section B below, for reference.
3. Enter logarithmic and decibel values in section C below, positive values in the plus column and negative values in the minus column. For example, if $-V_{0(dB)}$ as given by Figs. 4 through 9 is negative, then $-V_{0(dB)}$ is positive and goes in the plus column. For C_B, see Figs. 1 through 3. For definitions of the range factors, see Eq. (13).

Radar antenna height: h = ft. Target elevation angle: θ = 0.5°. (See Fig. 13.)

A. Computation of T_s:

$T_s = T_a + T_r + L_r T_e$

(a) Compute T_a.
For T_{tA} T_{ta} = 290 and T_g = 36 use Eq. (37a).
Read T_a' from Fig. 11.
$L_{a(dB)}$: 2.0 L_a: 1.585
$T_a = (0.876\,T_a' - 54)/L_a + 290$
T_a = 234 °K

(b) Compute T_r using Eq. (40).
For T_{tr} = 290 use Table 1.
$L_{r(dB)}$: 2.5 T_r = 226 °K

(c) Compute T_e using Eq. (41) or using Table 1.
$F_{n(dB)}$: 4 T_e: 438 °K
L_r: 1.778 $L_r T_e$ = 779°K

Add. T_s = 1239°K

B. Range Factors		C. Decibel Values	Plus (+)	Minus (-)
$P_{t(kW)}$	160	10 log $P_{t(kW)}$	22.0	·
$\tau_{\mu sec}$	60	10 log $\tau_{\mu sec}$	17.8	·
G_t	1122	$G_{t(dB)}$	30.5	·
G_r	1122	$G_{r(dB)}$	30.5	·
$\sigma_{(sq\,m)}$	1	10 log σ	—	—
f_{MHz}	1125	-20 log f_{MHz}	·	61.0
T_s (°K)	1239	-10 log T_s	·	30.9
V_0	4 pulses	$-V_{0(dB)}$	·	8.5
C_B	—	$-C_{B(dB)}$	·	—
L_t	2.0 dB	$-L_{t(dB)}$	·	2.0
L_p	1.6 dB	$-L_{p(dB)}$	·	1.6
L_x	2.2+3.0-9.0	$-L_{x(dB)}$	3.8	·
Range-equation constant (40 log 1.292)			4.45	
4. Obtain the column totals →			109.1	104.0
5. Enter the smaller total below the larger →			104.0	·
6. Subtract to obtain the net decibels (dB) →			+5.1	- ·

7. In Table 2 find the range ratio corresponding to this net decibel (dB) value, taking its sign (±) into account. Multiply this ratio by 100. This is R_0 → 134
8. Multiply R_0 by the pattern-propagation factor F = 1.56 (see Eqs. (42) through (65) and Figs. 12 through 19): $R_0 \times F = R'$ → 209
9. On the appropriate curve of Figs. 21 and 22 determine the atmospheric-absorption loss factor, $L_{a(dB)}$, corresponding to R'. This is $L_{a(dB)(1)}$. → 2.3
10. Find the range factor δ_1 corresponding to $-L_{a(dB)(1)}$ from the formula δ = antilog $(-L_{a(dB)}/40)$ or by using Table 2. → 0.876
11. Multiply R' by δ_1. This is a first approximation of the range R_1. → 183
12. If R_1 differs appreciably from R', on the appropriate curve of Figs. 21 and 22, find the new value of $L_{a(dB)}$ corresponding to R_1. This is $L_{a(dB)(2)}$. →
13. Find the range-increase factor (Table 2) corresponding to the difference between $L_{a(dB)(1)}$ and $L_{a(dB)(2)}$. This is δ_2. →
14. Multiply R_1 by δ_2. This is the radar range in nautical miles, R. →

Note: If the difference between $L_{a(dB)(1)}$ and $L_{a(dB)(2)}$ is less than 0.1 dB, R_1 may be taken as the final range value, and steps 12 through 14 may be omitted. If $L_{a(dB)(1)}$ is less than 0.1 dB, R' may be taken as the final range value, and steps 9 through 14 may be omitted. (For radar frequencies up to 10,000 megahertz, correction of the atmospheric attenuation beyond the $L_{a(dB)(2)}$ value would amount to less than 0.1 dB.)

(C) Fig. 13 -- Detection range calculation worksheet completed for Mode 2 (rain/chaff) waveform; 0.5 P_d, 10^{-8} P_{fa} on a 1-m^2 target

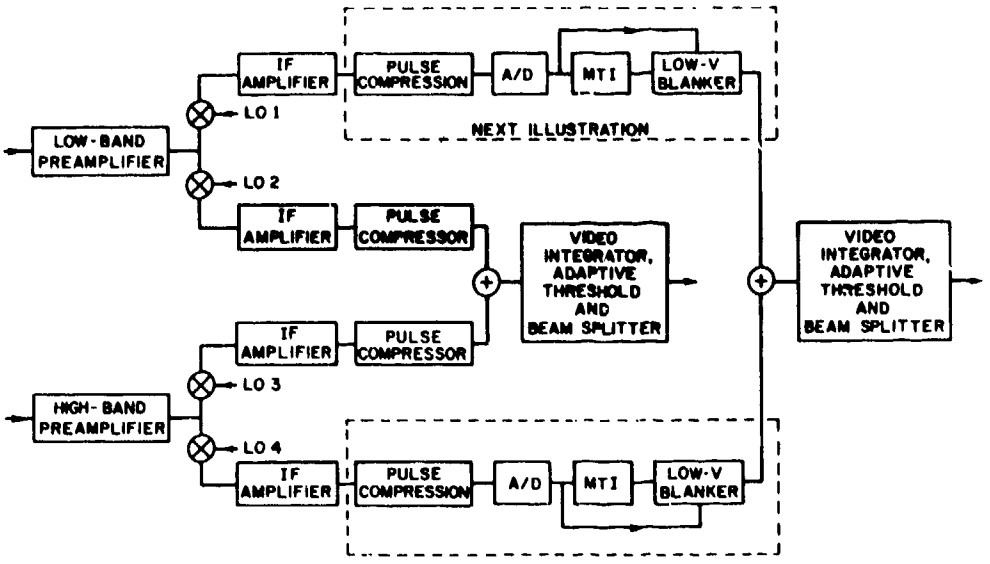

(C) Fig. 14 — Receiver-signal processor for 2-D radar

(C) All processing involving velocity filtering is done in the two outer signal channels shown in Fig. 14. After compression to a pulse length of 0.5 μs, signals in these channels are digitized and undergo velocity filtering to remove clutter returns prior to addition of the signals from the two bands. Pulse compression is performed prior to velocity filtering to permit use of the low-velocity target blanker described below.

(C) The section of Fig. 14 outlined by the dashed lines is expanded and elaborated in Fig. 15. This section is identical for both the low and high bands.

(C) The clear-sky MTI waveform (3-pulse bursts) is processed by the circuits shown in the lower half of Fig. 15. When the radar is in the clear-sky mode (Mode 1), the three switches in Fig. 15 are in the down position. The 10-μs pulses are compressed to 0.5 μs by the 20:1 pulse compressor. "I" and "Q" signals from the phase detector are digitized, and samples of these signals are extracted for comparison with the velocity-filtered signals in the low-velocity blanker circuit. The operation of this circuit will be explained in more detail in connection with Fig. 16. Suffice it to note here that the circuit is used to eliminate returns from fixed targets so large that they exceed the cancelation capability of the MTI processor. The 3-pulse canceler following the A/D converter is adjusted so that its notch is centered on the relative velocity of surface clutter (sea or land).

(C) When the radar is operated in the rain/chaff mode (Mode 2), the switches in Fig. 15 are placed in the up position. The 60-μs pulses are compressed to 0.5 μs in the 120:1 pulse compressor and go through the same phase detector, A/D converter, and 3-pulse canceler used to process the clear-sky signals. The Mode 2 signals then are processed in a second 3-pulse canceler for which the velocity notch is set at the mean velocity of the rain or chaff or both. The output of this canceler is fed into an 8-point FFT velocity filter.

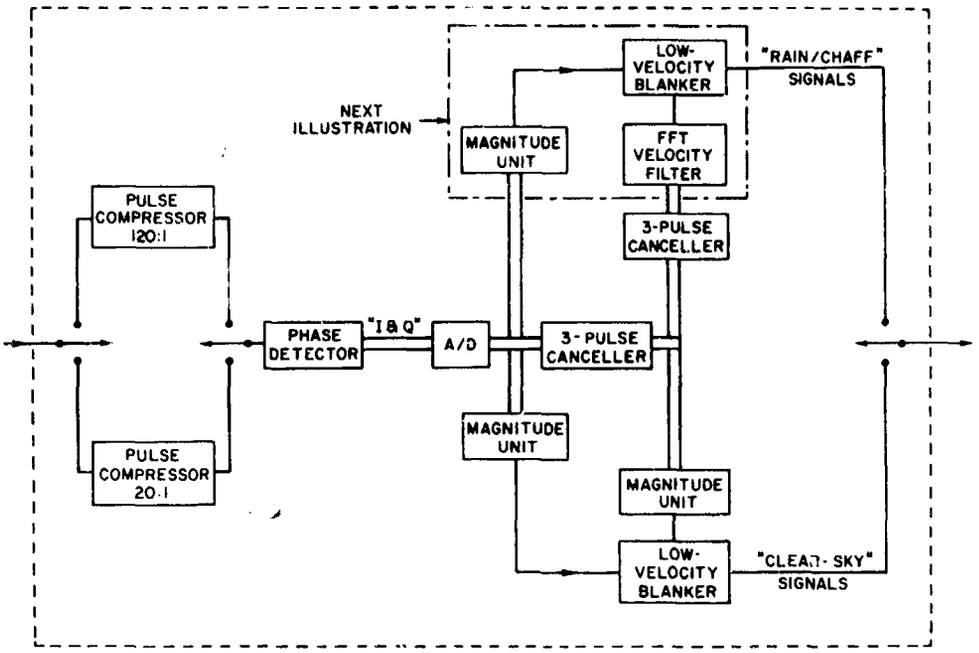

(C) Fig. 15 — Block diagram of velocity filtering channels

This filter and the low-velocity blanker associated with the Mode 2 processor are shown in more detail in Fig. 16.

(C) A shift register is used as the delay unit between each of the eight inputs to the FFT processor. Each of these shift registers provides a delay equivalent to the interpulse spacing. Outputs from the FFT processor are separated into eight doppler bands, each covering one-eighth of the range of dopplers from zero to the PRF. As indicated in Fig. 12, the PRF is switched between two values (typically 954 and 937 pps) on alternate 14-pulse sequences. This is done to resolve range ambiguities resulting from using a PRF corresponding to one-half the instrumented range. Detection occurs in the magnitude units on each of the eight doppler filters. A range-extent gate on each filter output acts to gate out a signal if it exists in more than two adjacent range bins. The assumption is that targets which extend through more than two range bins are clutter. The outputs from the velocity filter not blanked by the range extent gates are summed to a single output.

(C) In the upper signal channel in Fig. 16, digitized signals that have not undergone MTI processing are detected and then attenuated. The attenuation applied is approximately 3 dB less than the cancelation ratio achieved by the MTI cancelers against stationary objects. This attenuated signal is then compared with detected signals emanating from the velocity filters. If the magnitude of a signal from the unprocessed channel exceeds that of one from the processed channel (both occurring at the same range), the low velocity gate blanks the signal. The assumption which is the basis for this action is that any target with a significant radial velocity component will produce a larger signal in the MTI channel

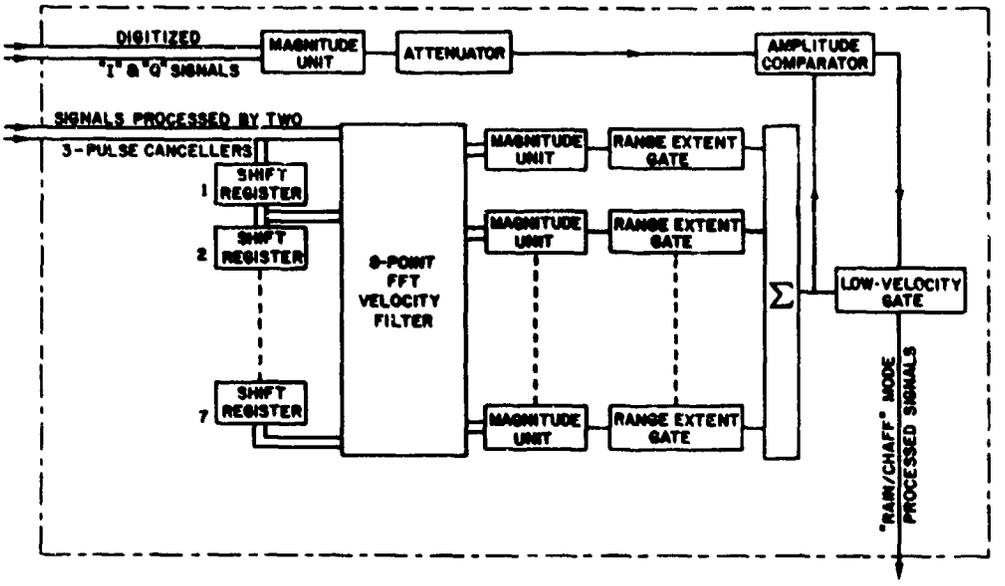

(C) Fig. 16 — Final stage of velocity filter and low-velocity blanker

than it will in the unprocessed channel. As previously noted, the function of the low-velocity blanker channel is to remove fixed point clutter returns, when their magnitude exceeds the cancelation capability of the MTI processor.

(C) To summarize, the signal processing performed in Mode 1 includes pulse compression and video integration of the long-range pulses, and pulse compression, 3-pulse canceler MTI processing, and video integration of the clear-sky MTI waveform. Mode 2 (rain/chaff) processing includes pulse compression, two stages of 3-pulse cancelers with offset clutter notches, FFT velocity filtering with blanking of range-extended targets, and video integration. Automatic target detection is provided in both modes.

Data Processing

(C) Data processing includes azimuth beam splitting, correlation of detections with track files, generation of track vectors for detected targets, and maintenance of tracks on multiple targets.

(C) After signal processing (pulse compression, MTI, and CFAR) is carried out in the two individual radar channels, the outputs from those signal processing channels are combined for video integration, adaptive thresholding, and automatic detection. The automatic detection function is combined with the azimuth beam-splitting function, and this area constitutes the interface between what is generally considered signal processing and what is considered data processing.

(C) A moving-window digital video integrator [8] will be used to add the returns from pulses transmitted within a beamwidth. The number of pulses per beamwidth varies as a function of the transmitted frequency, of course, since the azimuth beamwidth varies from 2.4° to 3.5° over the band. The moving-window integrator will be implemented to combine the number of pulses which are transmitted in the widest (low-frequency) beamwidth. The number of outputs from the signal processor also varies with the operating mode. Only two outputs per beamwidth are available in Mode 2, while four to six are available in both the MTI and long-range channels in Mode 1. Thus, in Mode 1, the moving-window integrator will be implemented for six samples, whereas in Mode 2 it will be implemented for two samples. Because of the long intervals between outputs from the MTI processor, random-access memory (RAM) units will be used as the integrator storage elements rather than shift registers. The interval between MTI outputs in Mode 2 is approximately 14.7 ms, and that in Mode 1 is 6.1 ms.

(U) The threshold-crossing azimuth-position estimator measures the length of time during which the detection threshold is exceeded and subtracts a fixed bias to determine the azimuth position of a target. If θ_1 is the azimuth at which the detection threshold is first exceeded and θ_2 the azimuth at which the integrated signal (output from the moving window integrator) drops below the threshold, the estimate of the target's azimuth is

$$\theta_t = \theta_1 + 1/2(\theta_2 - \theta_1) - \theta_B$$

where θ_B is the fixed bias. The value of θ_B is $N\Delta\theta/2$, where N is the number of samples combined in the moving-window integrator (the number of samples available within the 3-dB antenna beamwidth) and $\Delta\theta$ is the azimuth increment through which the antenna moves between samples.

(C) In Ref. 8, a calculation is made of the position-estimate accuracy achievable with a "small number" of samples (eight in the case for which the calculation is made) as a function of signal-to-noise (S/N) ratio. For a S/N ratio of 6 dB, the predicted rms value of the position measurement error is 0.113 beamwidth. Since there are six samples available for beam splitting in Mode 1 for SENRAD, it can be assumed that the position measurement accuracy will be comparable. At the lowest frequency beamwidth of 3.5°, this translates to an rms error of 0.39°. Since only two samples are available in Mode 2 operation, the position measurement error is expected to be greater, although a precise analysis has not been made. This error is a price that must be paid for detecting targets in rain and chaff at long ranges.

(U) Detections and position measurements are compared with the current track file. If a target falls within a correlation cell of a target currently in the track file, it is treated as an update of that track. If a detection cannot be correlated with a current track, it is considered as a tentative new track. After a number of detections of a new target are made, a velocity vector is generated for it and it is entered in the track file.

(U) Updates of target position measurements and track data are transmitted to displays at various user stations, including command and control, Combat Air Patrol and strike control, and weapon control.

Calculated Performance

(U) In this section, calculated performance of the 2-D radar in terms of detection sensitivity and performance in clutter environments is presented. Vertical-plane coverage diagrams are used to illustrate sensitivity.

(C) Figure 2 shows an outline of the volume in which a 1-m^2 target would be detected by the long-range waveform of Mode 1 with 0.5 probability of detection P_d and 10^{-8} probability of false alarm P_{fa}. In the calculation, the single-pulse S/N ratio required for detection of a Swerling Case 2 target for the stated P_d and P_{fa} was assumed. This assumption can be made because the pulse-to-pulse, frequency-agile operation effectively transforms the fluctuation characteristics of slowly fluctuating Case 1 targets to exhibit the rapidly fluctuating Case 2 characteristics. Thus, the graph applies to either Case 1 or Case 2 targets. At each elevation angle, the maximum response achieved on any one of four transmitted frequencies is plotted. Thus, the detection ranges shown are somewhat conservative in that no account is taken of noncoherent integration of pulses at different frequencies.

(C) When the receivers are implemented as shown in Fig. 14, the range sweep for the long-range waveform can be instrumented to 490 n.mi. This capability is based on the assumption that the MTI pulse burst is transmitted at a frequency different from that of the preceding long-range pulse. Thus, targets of sufficiently large cross section could be detected at ranges to 490 n.mi. if the range sweep were made that long. This feature might be of some value in detecting long-range missiles with a high trajectory. Figure 17 shows the detection envelope against a 7-m^2 target. The scale change between Figs. 2 and 17 should be noted.

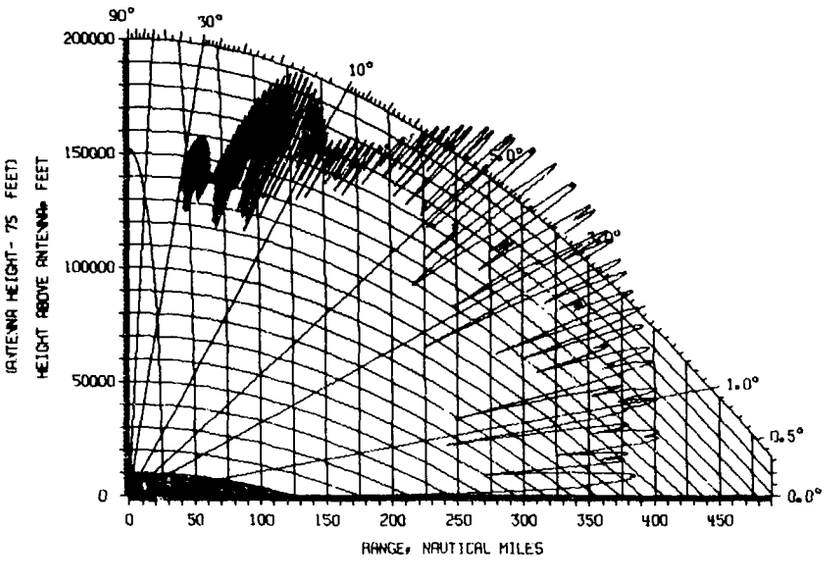

(C) Fig. 17 — Range-hieght coverage on a 7-m^2 target
(Mode 1, long-range waveform)

(C) A similar vertical-plane coverage diagram for the MTI waveform of Mode 1 is shown in Fig. 18. This chart is for a 1-m^2 target. It should be remembered that the MTI system is implemented only to 80 n.mi. for this mode.

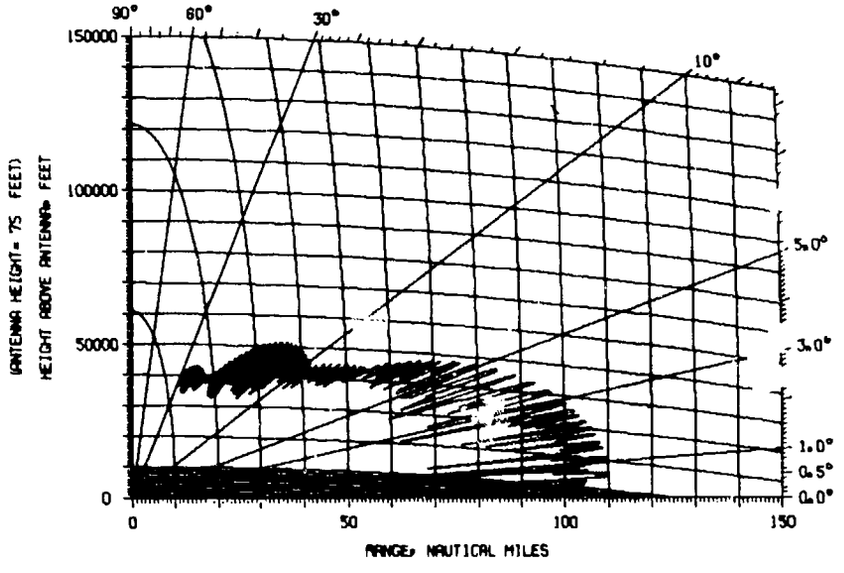

(C) Fig. 18 — Range-height coverage on a 1-m^2 target (Mode 1, MTI waveform)

(C) The sensitivity chart for Mode 2 operation is shown in Fig. 19, for a 1-m^2 target. This mode is instrumented to a range of 160 n.mi.

(C) Sea clutter does not present a significant problem for this radar. In a state 5 sea, an improvement factor of only 4.7 dB will permit detection of a 0.1-m^2 target with 0.9 P_d and 10^{-8} P_{fa}. This detection capability will exist from a minimum range of 5 n.mi. to the maximum range at which sea clutter is visible under normal propagation conditions.

(U) If a land clutter model is assumed in which the backscatter coefficient is constant with increasing range to a range of 30 n.mi. and decreases beyond 30 n.mi. because of obscuration due to earth's curvature, the most difficult range at which to detect targets in the land clutter environment is at 30 n.mi. If the 95th percentile value of the backscatter coefficient σ° is taken to be -18 dB, the improvement factor required for 0.9 P_d on a 0.1-m^2 target is 55 dB.

(C) Figure 20 shows the theoretical improvement factor provided by the Mode 1 3-pulse canceler as a function of the clutter-spectrum standard deviation. The maximum expected value of the standard deviation of the spectrum for sea clutter, considering a maximum sea roughness defined by sea state 5, is 2.3 knots [9]. Since, as was noted above, only a 4.7-dB improvement factor is required in sea state 5, it is obvious from Fig. 20

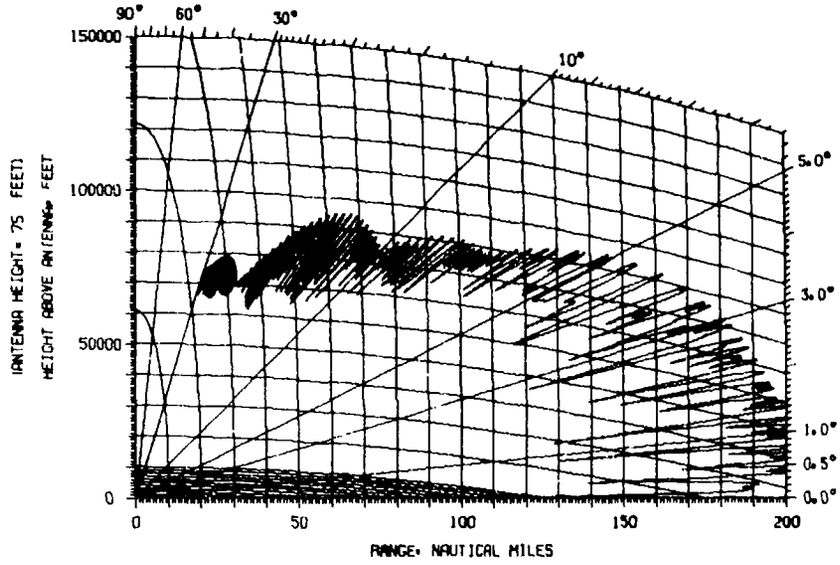

(C) Fig. 19 — Range-height coverage on a 1-m^2 target (Mode 2)

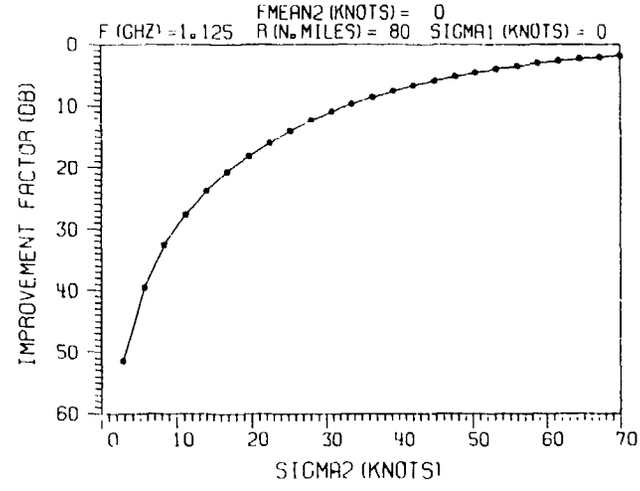

(U) Fig. 20 — Theoretical improvement factor of 3-pulse canceler vs standard deviation of the clutter spectrum

that the 3-pulse canceler will deal adequately with sea clutter. The maximum-expected-spectrum standard deviation for land clutter with windspeeds to 50 knots is less than 0.7b knots at L-band frequencies [9]. The calculated improvement required to cancel 95th percentile land clutter is 55 dB. Extrapolating the curve in Fig. 20 shows that if system stabilities are sufficiently good this value is theoretically achievable.

(C) Figure 6, which was used to demonstrate the advantages of wideband frequency agility in eliminating blind speeds, shows the response vs target velocity curve for the 3-pulse canceler when the target is illuminated by four widely spaced frequencies during each antenna scan. The chart covers only 2,000 knots; the first true blind speed occurs at approximately 60,000 knots.

(C) Preliminary calculations have been made of the Mode 2 performance against various levels of rain and chaff clutter. Figure 21 shows the calculated performance of the three-stage MTI system as a function of the standard deviation of the rain or chaff velocity spectrum [10]. These curves were based on assumed values of the standard deviation of surface clutter (5 knots) and for the mean velocity of the volume clutter (29 knots). The 5-knot value of standard deviation for area clutter is conservative for any expected land or sea clutter environments. The 29-knot mean velocity chosen for the volume clutter is arbitrary; however, it is considered typical. The result of assuming different values of mean velocity would be to alter the responses of some of the eight outputs from the FFT velocity filter without causing major changes in the overall performance. The circled dots indicate the improvement factor against volume clutter due to the second 3-pulse canceler alone. The solid lines, numbered 0 to 7, show the improvement factor of the total MTI system at the eight outputs of the FFT velocity filter. These curves were calculated for the midband frequency. Curves marked with short vertical lines show the improvement factor against surface clutter at the outputs of the MTI system. Since in most channels, this improvement factor is greater than 60 dB (the maximum shown), only two lines appear on the chart.

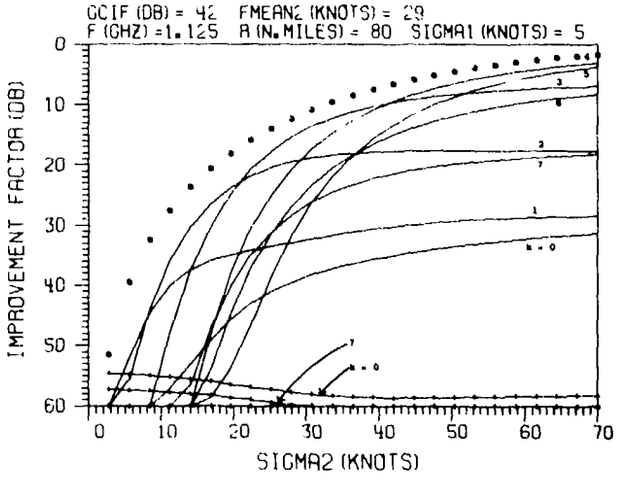

(C) Fig. 21 — Calculated performance of 3-stage MTI system vs standard deviation of clutter spectrum

(C) Several curves are plotted in Fig. 22 to show the improvement factors required for 0.5 P_d at 10^{-8} P_{fa} in the following clutter environments:

a. 1 mm/hr rain
b. 4 mm/hr rain
c. 16 mm/hr rain
d. 10 $m^2/(n.mi.)^3$ chaff
e. 100 $m^2/(n.mi.)^3$ chaff
f. 1000 $m^2/(n.mi.)^3$ chaff.

The rain and/or chaff are assumed to be uniformly distributed from the surface of the earth to an altitude of 25,000 ft. and to not exist above that altitude. The break in the curves between ranges of 80 and 90 mi is due, of course, to the fold-over of near-range clutter onto the range bins beyond 80 mi. The shadowing of a large portion of the clutter at those ranges, due to earth's curvature, causes the falloff of the required improvement factor at the longest ranges. If clutter does not exist at near ranges, the improvement factor required at long ranges will increase only about 1 dB above its value at 80 n.mi.

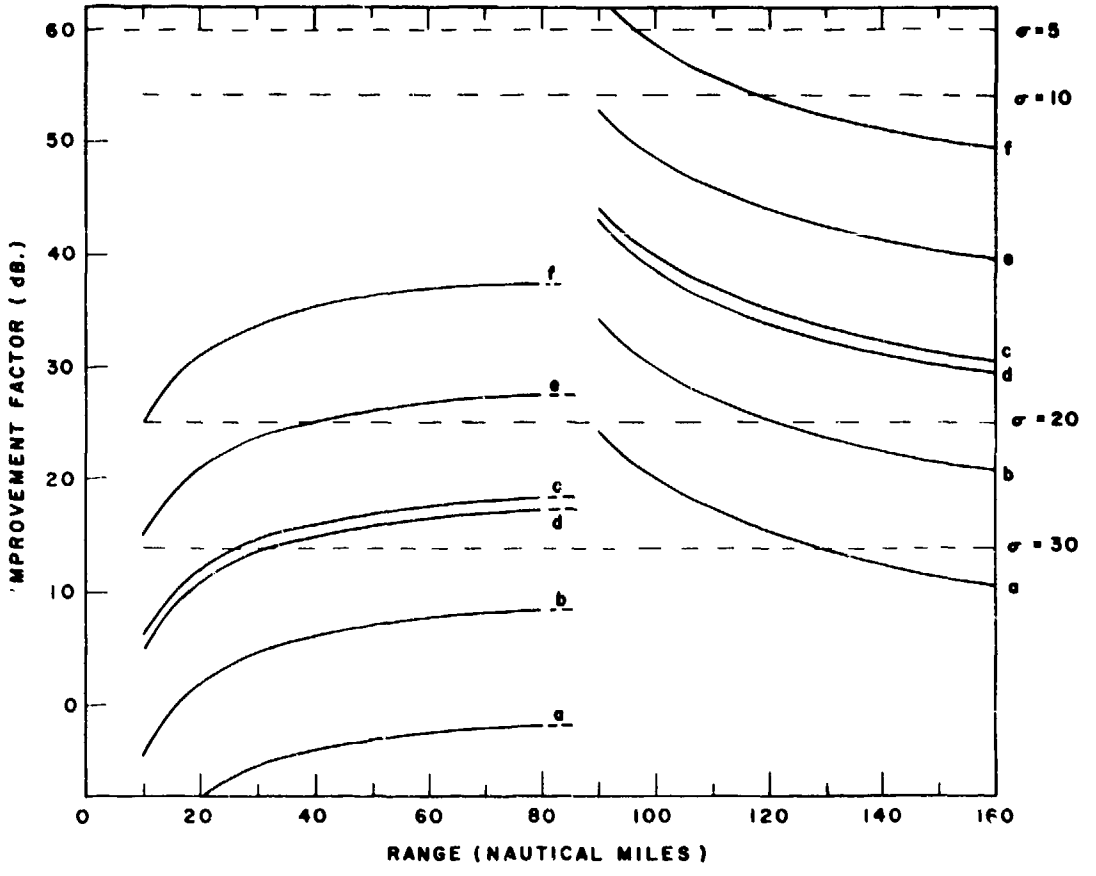

(C) Fig. 22 — Required and predicted MTI improvement factor for several clutter environments to achieve 0.5 P_d on a 1-m^2 target

(U) Also plotted on Fig. 22 are the calculated improvement factors that will be achieved by the MTI system, with several assumed values of standard deviation σ of the clutter spectrum illuminated by the radar. These values of improvement factor are extracted from Fig. 21, excluding the first three of the eight filters in the FFT filter bank.

(U) These calculations are considered preliminary and represent a conservative design approach. This assessment is made because of the following considerations. The improvement factors were calculated on the basis of a Gaussian distribution of clutter velocities. In reality, the velocity spectrum will be truncated by the upper altitude limit of chaff or rain and by the horizon. Thus, when a wide fan beam is used in the elevation plane, the clutter extent in the antenna pattern will be limited to a relatively narrow portion in which the field strength remains almost constant. For that reason, something approaching a uniform truncated distribution might be more appropriate than the Gaussian distribution assumed. A second point is that no effort was made to optimize the combination of three stages of the MTI system, although the individual stages were optimized. These considerations tend to make the calculations presented in Figs. 21 and 22 somewhat pessimistic.

DESCRIPTION OF THREE-DIMENSIONAL RADAR

(U) The 3-D radar described here is intended to meet the need which exists on certain ship types for tracking targets in three dimensions (range, azimuth, and height). This radar uses a rotating planar array antenna and provides track-while-scan operation.

(C) Elevation angle information on airborne targets is not of much value at very long ranges since the total elevation angle defined by the horizon and the upper altitude limit for these targets is small. That is, for reasonable apertures, the elevation beamwidth is comparable to the total elevation sector of interest at ranges beyond 200 n.mi. For that reason, and more importantly, for reasons of economy in cost and weight, the primary mode of the radar is instrumented only to a range of 125 n.mi. Another mode is available which provides elevation information to a range of 250 n.mi., but only in an elevation sector of approximately 6°.

(C) Some of the major features of the 3-D radar are listed below.

Frequency	850-1400 MHz
Antenna	Array, phase-scanned in elevation, coverage from 0 to 70° with monopulse in azimuth and elevation
Data rate	4s (6s in rain or chaff)
Transmitter	Transistor row amplifiers.

Figure 23 is block diagram of the 3-D radar.

(C) Associated with each row of radiators of the array antenna are a multiple-transistor power amplifier, two low-noise preamplifiers, and two low-power phase shifters. A pulse

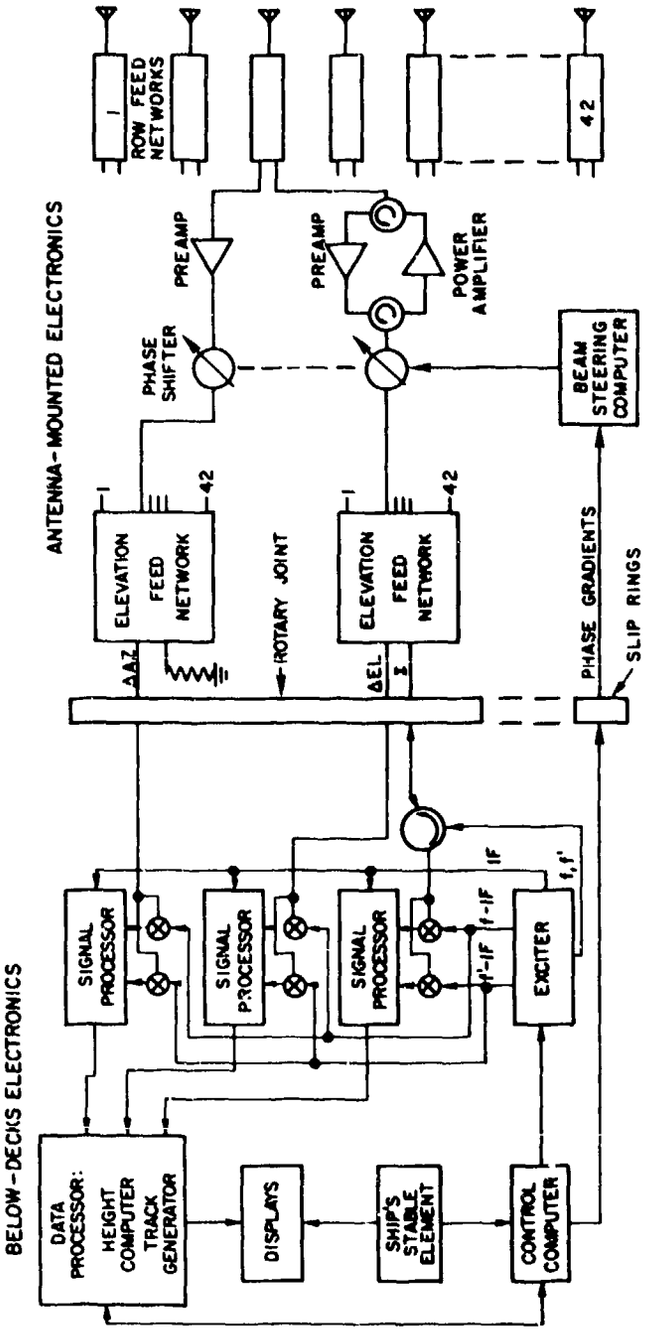

(C) Fig. 23 — Three-dimensional radar system

at the radio frequency to be transmitted is generated by the exciter, passes through a duplexing circulator, through one channel of a three-channel rotary joint, and into the sum port of a low-power 1:42 elevation feed network. Each of the 42 outputs from the elevation feed passes through a low-power phase shifter, where elevation steering phases are applied, and drives a power amplifier; each of these amplifiers in turn drives one row of the array.

(C) Received signals are combined by the row feed networks to form a sum signal and an azimuth difference signal at each row. Each of these signals is amplified by a low-noise preamplifier and is phase shifted for elevation steering. The 42 azimuth difference signals are then summed in an elevation feed to form the total azimuth difference signal. The 42 sum signals are combined in a second elevation feed to form the total sum signal and the elevation difference signal. The sum, azimuth difference, and elevation difference signals pass through the three channels of the rotary joint to the signal processors. The need for two mixers at the input to each signal processor will become apparent in a later discussion of waveforms. The signal processors perform the functions of pulse compression and MTI and CFAR processing. Target reports go to the data processor where position estimates are made and tracks generated.

(C) A control computer performs the functions of frequency selection, mode control, and phase gradient generation for electronic beam stabilization and elevation steering. The beam-steering computer, which generates the phase commands for each of the individual phase shifters, is located on the rotating antenna. Thus, it is only necessary to pass a phase gradient command through the slip rings to the beam-steering computer.

(U) No mechanical stabilization is required for this antenna, and no significant position measurement errors will occur as a result of the line-of-sight (LOS) stabilization of a pencil-beam pattern. This is contrary to the case when LOS stabilization is used with a fan-beam pattern, which leads to significant azimuth position measurement errors. The difference in the two cases is, of course, that with a 3-D pencil beam radar the height of a target can be determined and thus the correct azimuth can be calculated, regardless of the plane in which the beam is scanned and stabilized.

Transmitter

(C) The proposed transmitter configuration for the 3-D radar has individual final power amplifiers driving each row of the array. Each of these final amplifiers consists of multiple transistors. The dc power supplies for the row amplifiers are below deck to reduce weight on the rotating antenna. This arrangement requires that dc current of the order of 350 A at 28 V be passed through slip rings to the antenna.

(C) The General Electric Co., Syracuse, N.Y., has demonstrated with a transistor module the bandwidth necessary for this application [11]. Curves showing bandwidths at the 1- and 2-dB power points of this module are presented in Fig. 24. This module consists of one transistor driving two in parallel. If a 42-W power output and a 1.5-dB combining loss are assumed, 20 such modules will be required to develop the required pulse power of 595 W for one row. Thus, approximately 70 transistors, including driver stages, are required for each of the 42 row transmitters, or a total of 2,940 for the entire array.

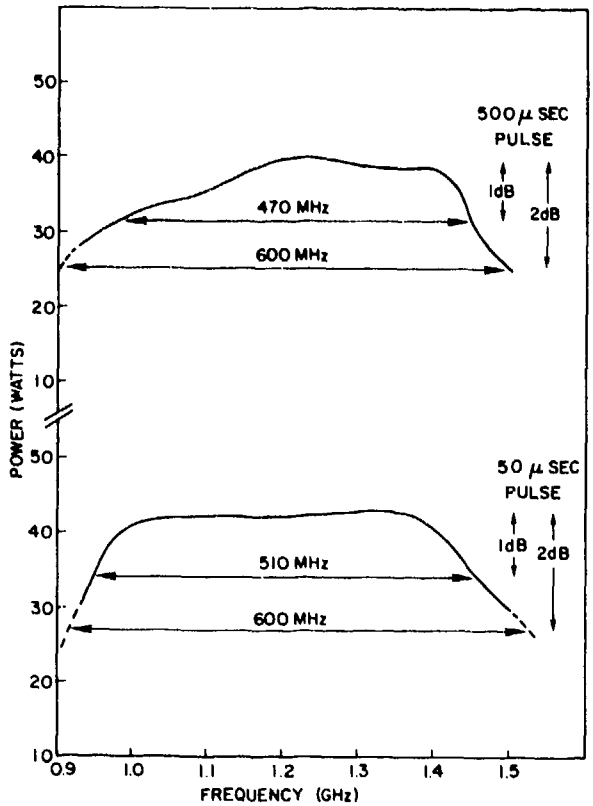

(U) Fig. 24 — Power output of GE transistor module vs frequency for two pulse widths [11]

(C) Some of the characteristics of the individual row transmitter and the corresponding quantities for the entire array are listed below.

	Row Transmitter	Array Transmitter
Pulse power	600 W	25 kW
Maximum pulse length	400 μs	400 μs
Maximum average power	68.4 W	2850 W
Number of transistors	70	2940

(C) Figure 25 is a diagram of a row amplifier. An input power of 1 W is amplified and divided into two portions, and each portion is further amplified to a 60-W level. Each signal drives a series power combiner of 10 modules, and the outputs of the two series combiners are added to provide the 600-W pulse power for one row of the array. The inset on Fig. 25 shows the construction of one of the 20 amplifier modules. It consists of one 4-cell transistor driving two 8-cell transistors.

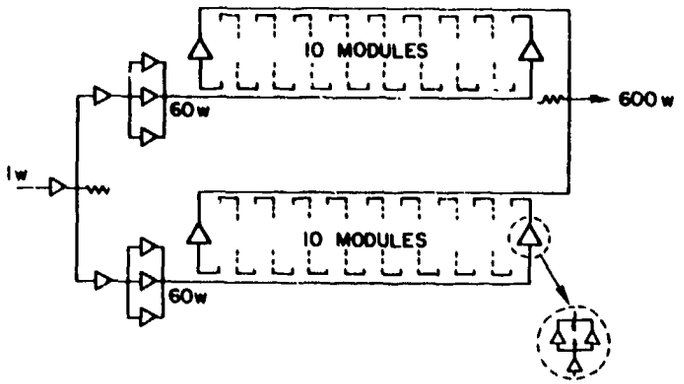

(C) Fig. 25 — Row power amplifier with inset of 3 transistor module

(C) An alternative would be to drive the entire array with a below-deck transmitter incorporating the wideband TWT discussed earlier in connection with the 2-D radar. This approach would result in a significant decrease in the weight of the antenna, since the power amplifiers would be removed from that structure. There are, however, other considerations which favor the solid state row transmitter.

1. If a single, high-power transmitter is used to drive the entire array, it is necessary to use high-power phase shifters for elevation beam steering. These are more difficult to develop and somewhat less reliable than the low-power devices which can be placed *ahead* of the row transmitters.

2. The overall efficiency of the transmitter-antenna combination is greater when the row transmitter approach is used. This is because reduced transmission line losses are incurred when the transmitters are placed in the antenna feed structure.

3. Transistor amplifiers are "RF-modulated" devices; i.e., they require no modulation of the bias voltage. Accordingly they are much more attractive for a scanning beam 3-D radar transmitter than is a large tube, which requires modulation of the beam current. Efficient use of a 3-D radar which maintains a constant detection sensitivity at a constant altitude line requires "programming" of the transmitted energy as a function of elevation scan angle. For example, if the elevation sector of interest is from the horizon to an elevation angle of 70°, with a maximum altitude of 100,000 ft, most efficient use of radar time and energy requires that both the pulse energy and interpulse period be varied as a function of elevation angle. It is much easier to achieve this type of power programming with RF-modulated amplifiers than with large tubes and their associated modulators, which are inherently inflexible.

(U) As has been mentioned earlier, the primary disadvantages of the row transmitter concept are the added weight of the antenna and the necessity for carrying relatively large dc currents through slip rings.

(U) Some alternative transmitter configurations using transistor amplifiers which might be considered for a rotating, 3-D phase-scanned antenna are

1. A below-deck transmitter, in which the outputs of a sufficient number of transistors are combined to provide the total radiated power.

2. Row transmitters with the associated dc power supplies located on the antenna.

3. Row transmitters with the dc power supplies below deck.

4. An approach with one module per radiator, in which the amplifiers are distributed throughout the entire array.

(U) A tradeoff comparison was made of these alternatives in connection with an earlier design study [12]. The conclusion was that alternative 3 provides the best compromise between antenna weight and total system cost.

Antenna

A conceptual drawing of the 3-D antenna is Fig. 26. The same type of open construction as described earlier for the 2-D antenna is used here, with printed board azimuth feeds and printed dipole radiators. A significant difference in the two antennas is the cluster of row transmitters, preamplifiers, and phase shifters along the vertical centerline of the antenna. These components add significantly to the weight of this antenna, of course. A second significant difference is that no mechanical stabilization of the antenna is required. Electronic LOS stabilization is provided by the phase shifter, together with elevation beam steering. The radiators are identical to those used in the 2-D antenna.

(C) Characteristics of the antenna are listed below.

Array size	15 ft high by 15 ft wide
Number of dipoles	1008
Number of phase shifters	84
Azimuth beamwidth	
850 MHz	4.8°
1400 MHz	2.9°
Elevation beamwidth	
Transmit	
850 MHz	4.0°
1400 MHz	2.4°
Receive	
850 MHz	4.8°
1400 MHz	2.9°

Gain	
850 MHz	32 dB
1400 MHz	36.3 dB
Peak sidelobes (Receive)	-25 dB
Polarization	Horizontal
Monopulse	Azimuth and elevation
Weight	≈5000 lb.

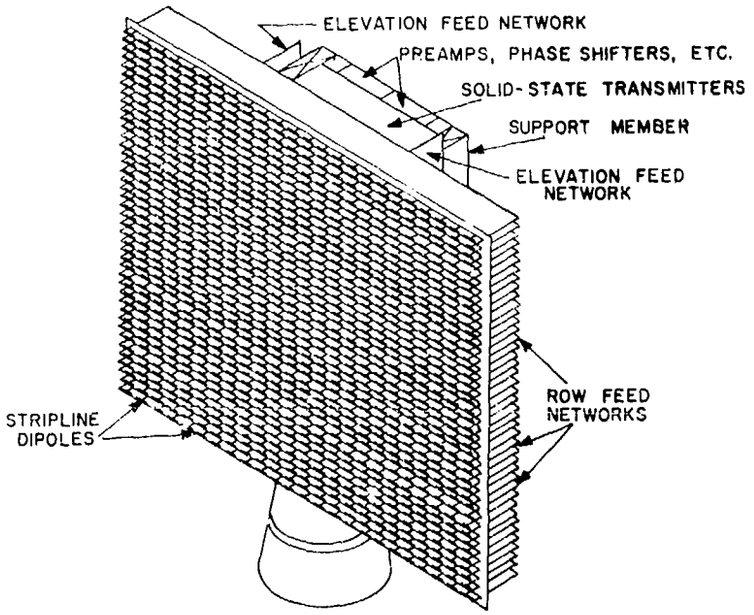

(U) Fig. 26 — Conceptual drawing of 3-D antenna

Modes of Operation

(C) Four selectable modes of operation are described in the following paragraphs: Mode 1, an intermediate-range, clear-sky mode (considered the primary mode), Mode 2, a rain/chaff mode; Mode 3, a long-range mode; and Mode 4, a fan-beam search mode. A variation of the intermediate range mode is used for heavy rain or chaff.

Intermediate-Range Clear-Sky Mode (Mode 1)

(C) This is the mode in which the radar is expected to be operated most of the time. The instrumented range is 125 n.mi. at 0° elevation, and coverage is maintained at an altitude of 100,000 ft to an elevation angle of 70°. The maximum pulse length used is

200 μs (at the lowest elevation angles) and this is compressed to 0.5 μs on reception. The maximum interpulse period is 1745 μs. Both the pulse length and the interpulse spacing are reduced as the beam is scanned to high elevation angles because of the reduced range sweep and reduced sensitivity required to maintain coverage at the 100,000-ft altitude line.

(C) If the environment is clear of chaff or heavy rainfall, the radar is operated in the clear-sky mode. In this mode, (Mode 1), MTI is implemented only in the lowest beam position and extends to the full instrumented range of 125 n.mi. A 3-pulse canceler is used to discriminate against land and sea clutter returns. Four 3-pulse groups are transmitted in the first beam position, the transmitted frequency being shifted after each group of three pulses. This shift of frequency is used, as indicated earlier, to force a noise jammer to spread his energy and to eliminate interference nulls and MTI blind speeds. The clear-sky mode waveform is shown in Fig. 27. With some beam broadening at the highest elevation angles, a 4-s data rate search of 360° in azimuth can be maintained with the waveform pictured here. A typical elevation-scan energy-management program is shown in Table 1. It will be noted that in the course of the elevation scan, the beamwidth, range sweep, number of pulses, and pulse lengths are varied.

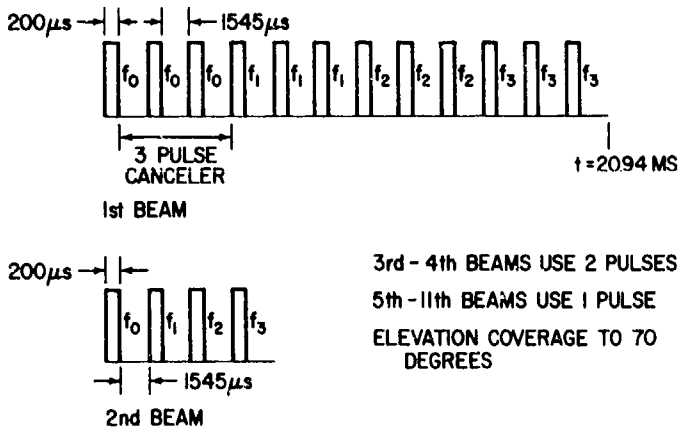

(C) Fig. 27 — Clear-sky mode (Mode 1) waveform for first two elevation beam positions

(C) With the 200-μs pulse length, the minimum range achievable is 16-20 n.mi. This is not considered a satisfactory minimum range. Therefore, at the end of each 200-μs pulse, the transmitted frequency is shifted to a different frequency f′ for 0.5 μs. The use of two mixers and two IF amplifiers in each receiver-processor chain, as shown in Fig. 23, permits simultaneous reception of both the f and f′ frequencies. The f′ frequency is used for detections in the range interval of 0.5 to 20 n.mi., and frequency f is used for detections from 20 to 125 n.mi. The offset of frequency f′ from frequency f must be small enough that the beam position is not materially changed with a single setting of the phase shifters. That is, since both frequencies must be received at the same time, it will not be possible to use different phase shifter settings.

(C) Table 1
Elevation Scan Program, Clear-Sky Mode

Elevation Angle (deg)	Range Sweep (n.mi.)	Pulses	τ (μs)	Time (ms)
1.6	125 n.mi.	12	200	20.9
4.9	125	4	200	7.0
8.2	125	2	200	3.5
11.5	87	2	100	2.3
16.5	66	1	100	0.9
23.1	45	1	50	0.6
29.7	32	1	50	0.4
39.6	24	1	10	0.3
52.5	23	1	10	0.3
66.0	18	1	10	0.2
				36.6

(C) In order to avoid confusion, the f′ frequency pulse segments are not shown on the waveform diagram. Suffice it to say that, at the end of each f_o pulse there is an f_o' pulse, at the end of each f_1 pulse an f_1' pulse, etc.

Rain/Chaff Mode (Mode 2)

(C) To detect small moving targets in rain or chaff, it is necessary to cancel more than three pulses in the MTI processor. This is because of the greater spectral spread of wind-blown rain and chaff compared to that of sea and land clutter. The wider filter notch required to suppress returns from clutter with a wide spectral spread necessitates the processing of a larger number of pulses [13]. For this mode (Mode 2), a 6-pulse canceler was chosen. Because these types of clutter may exist at all elevation angles, it is necessary to use the MTI throughout the elevation sector. This combination of requirements results in a further requirement to increase the data interval from 4 to 6s. Even so, there is not enough time to illuminate any but the first elevation beam position with more than one frequency. This position is illuminated with two groups of six pulses at two frequencies to help alleviate the interference null problem. Because it is not possible to utilize multiple frequencies at each beam position in this MTI mode, the interpulse spacings of the pulse groups must be staggered to reduce blind speed problems. A method of designing an optimized MTI filter of this type is described in Ref. 4.

(C) Figure 28 shows the waveform for the first elevation beam position. The remaining beam positions are illuminated with only one group of six pulses. To detect targets at ranges less than 20 n.mi., short pulses at different frequencies are added onto the end of each 200-μs pulse as described for the clear-sky mode.

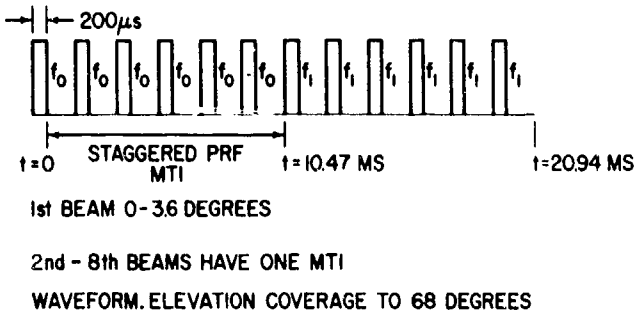

(C) Fig. 28 — Rain/chaff mode (Mode 2) waveform for first elevation beam position

(C) A typical elevation scan energy management program for the rain/chaff mode is shown in Table 2. By using beam broadening factors of 2 and 4 at higher elevation angles, an elevation scan to 70° can be achieved in 60 ms. This is the time available during a rotation in azimuth of 3.6° at a 10-rpm antenna scan rate. This scan would be completed in something just over the center frequency azimuth beamwidth of 3.53°. To assure azimuth coverage, it may be necessary to reduce the elevation coverage by one beam position.

(C) Table 2
Elevation Scan Program for Rain/Chaff Mode

Elevation Angle (deg)	Range Sweep (n.mi.)	Pulses	τ (μs)	Time (ms)
1.6	125	12	200	20.9
4.9	125	6	200	10.5
8.2	125	6	200	10.5
13.0	70	6	100	5.8
19.6	50	6	100	4.3
26.2	36	6	50	3.0
39.4	24	6	10	1.8
52.2	23	6	10	1.8
65.4	18	6	10	1.4
				60.0

(C) A range calculation work sheet for the intermediate-range modes is presented in Fig. 29. The calculation is made for 0.5 probability of detection with a 10^{-8} false alarm probability against a 1-m^2 target with Swerling Case 1 fluctuation characteristics. The calculation is made for the middle of the frequency band, and it predicts a detection range of 112 n.mi.

PULSE-RADAR RANGE-CALCULATION WORK SHEET

For use in conjunction with NRL Report 6930 (Dec. 1969). Based on Eq. (13), page 10, and associated auxiliary equations and curves as referenced below.

1. Compute the system input noise temperature T_s, following the outline in section A below.
2. Enter range factors known in other than decibel form in section B below, for reference.
3. Enter logarithmic and decibel values in section C below, positive values in the plus column and negative values in the minus column. For example, if $V_{0\,(dB)}$ as given by Figs. 4 through 9 is negative, then $-V_{0\,(dB)}$ is positive and goes in the plus column. For C_B, see Figs. 1 through 3. For definitions of the range factors, see Eq. (13).

Radar antenna height: h = ft. Target elevation angle: $\theta = 0.5°$. (See Fig. 13.)

A. Computation of T_s: $T_s = T_a + T_r + L_r T_e$

(a) Compute T_a.
For $T_{tg} = T_{ta} = 290$ and $T_g = 36$ use Eq. (37a).
Read T_a' from Fig. 11.
$L_{a(dB)}$: 1.6 L_a: 1.445
$T_a = (0.876\,T_a' - 254)/L_a + 290$
T_a = 175 °K

(b) Compute T_r using Eq. (40).
For T_{tr} = 290 use Table 1.
$L_{r(dB)}$: 1.6 T_r = 129 °K

(c) Compute T_e using Eq. (41) or using Table 1.
$F_{n(dB)}$: 4 T_e: 438 °K
L_r: 1.445 $L_r T_e$ = 633 °K

Add. T_s = 937 °K

B. Range Factors		C. Decibel Values	Plus (+)	Minus (−)
$P_{t\,(kW)}$	25	10 log $P_{t\,(kW)}$	14.0	.
$\tau_{\mu sec}$	200	10 log $\tau_{\mu sec}$	23.0	.
G_t	3535	$G_{t\,(dB)}$	35.5	.
G_r	2904	$G_{r\,(dB)}$	34.6	.
$\sigma_{(sq\,m)}$	1	10 log σ	—	—
f_{MHz}	1125	−20 log f_{MHz}	.	61.0
T_s (°K)	937	−10 log T_s	.	29.7
V_0	4 pulses	$-V_{0\,(dB)}$	.	9.1
C_B	—	$-C_{B\,(dB)}$		—
L_t		$-L_{t\,(dB)}$		1.6
L_p		$-L_{p\,(dB)}$		3.2
L_x		$-L_{x\,(dB)}$		3.0
Range-equation constant (40 log 1.202)			4.45	
4. Obtain the column totals →			111.6	107.6
5. Enter the smaller total below the larger →			107.6	.
6. Subtract to obtain the net decibels (dB) →			+4.0	− .

7. In Table 2 find the range ratio corresponding to this net decibel (dB) value, taking its sign (±) into account. Multiply this ratio by 100. This is R_0 → 126
8. Multiply R_0 by the pattern-propagation factor F = 1.0 (see Eqs. (42) through (65) and Figs. 12 through 19): $R_0 \times F = R'$ → 126
9. On the appropriate curve of Figs. 21 and 22 determine the atmospheric-absorption loss factor, $L_{\alpha(dB)}$, corresponding to R'. This is $L_{\alpha(dB)(1)}$. → 2.0
10. Find the range factor δ_1 corresponding to $-L_{\alpha(dB)(1)}$ from the formula δ = antilog $(-L_{\alpha(dB)}/40)$ or by using Table 2. → 0.8913
11. Multiply R' by δ_1. This is a first approximation of the range R_1. → 112
12. If R_1 differs appreciably from R', on the appropriate curve of Figs. 21 and 22, find the new value of $L_{\alpha(dB)}$ corresponding to R_1. This is $L_{\alpha(dB)(2)}$. →
13. Find the range-increase factor (Table 2) corresponding to the difference between $L_{\alpha(dB)(1)}$ and $L_{\alpha(dB)(2)}$. This is δ_2. →
14. Multiply R_1 by δ_2. This is the radar range in nautical miles, R. →

Note: If the difference between $L_{\alpha(dB)(1)}$ and $L_{\alpha(dB)(2)}$ is less than 0.1 dB, R_1 may be taken as the final range value, and steps 12 through 14 may be omitted. If $L_{\alpha(dB)(1)}$ is less than 0.1 dB, R' may be taken as the final range value, and steps 9 through 14 may be omitted. (For radar frequencies up to 10,000 megahertz, correction of the atmospheric attenuation beyond the $L_{\alpha(dB)(2)}$ value would amount to less than 0.1 dB.)

(C) Fig. 29 — Detection range calculation worksheet completed for Mode 1 waveform; 0.5 P_d, 10^{-8} P_{fa} on a 1-m^2 target

Long-Range Mode (Mode 3)

(C) A third mode is provided to permit detection and tracking of larger targets to ranges of 250 n.mi. at a 4-s data rate. In this mode, elevation coverage is provided only to 6.6° (2 beamwidths above the horizon). The pulse length is increased to 400 μs and the PRF reduced to keep the same average radiated power as in the intermediate-range mode. No MTI processing is provided in this mode, since it is intended primarily for targets beyond a range of 125 n.mi.

(C) The waveform transmitted is shown in Fig. 30. The solid pulses are transmitted in the lower beam position, and the dotted pulses are transmitted in the upper beam position. The radiated frequency may be changed on every pulse. Since that is the case, a target whose fluctuation characteristic is Swerling Case 1 (typical of aircraft targets) may be made to have the pulse-to-pulse fluctuation characteristic of a Case 2 target. The required S/N ratio for 0.5 P_d of a Case 2 target with a 10^{-8} P_{fa} is 1.3 dB less than for a Case 1 target [14]. A calculation of the detection range against a Case 2 target when the radar is in the long-range mode is shown in Fig. 31. The target size assumed in this calculation is 5 m^2, since it seems reasonable that targets of interest in the 125-250 n.mi. range sector are likely to be larger. Again, the calculation is made for the midband frequency, and predicts a detection range of 238 n.mi.

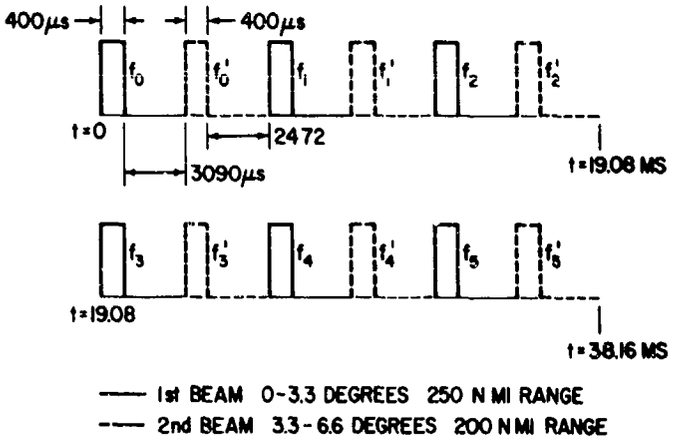

(C) Fig. 30 — Long-range mode (Mode 3) waveform

Fan-Beam Search Mode (Mode 4)

(C) A mode that takes advantage of the inherent flexibility of a phase-scanned antenna has been devised which will permit searching from the horizon to 70° elevation, to a range of 250 n.mi., and still provide height information and 3-D tracking on selected targets. A sufficient number of pulses are available in each azimuth beamwidth to permit reasonably good MTI processing. The fan beam used in this mode, designed for routine

PULSE-RADAR RANGE-CALCULATION WORK SHEET

For use in conjunction with NRL Report 6930 (Dec. 1969). Based on Eq. (13), page 10, and associated auxiliary equations and curves as referenced below.

1. Compute the system input noise temperature T_s, following the outline in section A below.
2. Enter range factors known in other than decibel form in section B below, for reference.
3. Enter logarithmic and decibel values in section C below, positive values in the plus column and negative values in the minus column. For example, if $V_{0(dB)}$ as given by Figs. 4 through 9 is negative, then $-V_{0(dB)}$ is positive and goes in the plus column. For C_B, see Figs. 1 through 3. For definitions of the range factors, see Eq. (13).

Radar antenna height: h = ft. Target elevation angle: θ = 0.5°. (See Fig. 13.)

A. Computation of T_s: $T_s = T_a + T_r + L_r T_e$	B. Range Factors		C. Decibel Values	Plus (+)	Minus (−)
(a) Compute T_a. For $T_{tg} = T_{ta} = 290$ and $T_g = 36$ use Eq. (37a). Read T_a' from Fig. 11. $L_{a(dB)}$: 1.6 L_a: 1.445 $T_a = (0.876\,T_a' - 254)/L_a + 290$ T_a = 175°K	$P_{t(kW)}$	25	10 log $P_{t(kW)}$	14.0	.
	$\tau_{\mu sec}$	400	10 log $\tau_{\mu sec}$	26.0	.
	G_t	3535	$G_{t(dB)}$	35.5	.
	G_r	2904	$G_{r(dB)}$	34.6	.
	$\sigma_{(sq\ m)}$	5	10 log σ	7.0	.
	f_{MHz}	1125	−20 log f_{MHz}	.	61.0
	T_s (°K)	937	−10 log T_s	.	29.7
	V_0	6 pulses	$-V_{0(dB)}$	.	6.5
	C_B	—	$-C_{B(dB)}$		—
	L_t		$-L_{t(dB)}$		1.6
	L_p		$-L_{p(dB)}$		3.2
	L_x		$-L_{x(dB)}$		3.0
(b) Compute T_r using Eq. (40). For $T_{tr} = 290$ use Table 1. $L_{r(dB)}$: 1.6 T_r = 129 °K	Range-equation constant (40 log 1.292)			4.45	
	4. Obtain the column totals →			121.6	105.0
	5. Enter the smaller total below the larger →			105.0	.
	6. Subtract to obtain the net decibels (dB) →			17.6	− .
(c) Compute T_e using Eq. (41) or using Table 1. $F_{n(dB)}$: 4 T_e: 436 °K L_r: 1.445 $L_r T_e$ = 633°K	7. In Table 2 find the range ratio corresponding to this net decibel (dB) value, taking its sign (±) into account. Multiply this ratio by 100. This is R_0 →				275
	8. Multiply R_0 by the pattern-propagation factor F = 1.0 (see Eqs. (42) through (65) and Figs. 12 through 19): $R_0 \times F = R'$ →				275
Add. T_s = 937°K					

9. On the appropriate curve of Figs. 21 and 22 determine the atmospheric-absorption loss factor, $L_{\alpha(dB)}$, corresponding to R'. This is $L_{\alpha(dB)(1)}$. → 2.5
10. Find the range factor δ_1 corresponding to $-L_{\alpha(dB)(1)}$ from the formula δ = antilog $(-L_{\alpha(dB)}/40)$ or by using Table 2. → 0.866
11. Multiply R' by δ_1. This is a first approximation of the range R_1. → 238
12. If R_1 differs appreciably from R', on the appropriate curve of Figs. 21 and 22, find the new value of $L_{\alpha(dB)}$ corresponding to R_1. This is $L_{\alpha(dB)(2)}$. →
13. Find the range-increase factor (Table 2) corresponding to the difference between $L_{\alpha(dB)(1)}$ and $L_{\alpha(dB)(2)}$. This is δ_2. →
14. Multiply R_1 by δ_2. This is the radar range in nautical miles, R. →

Note: If the difference between $L_{\alpha(dB)(1)}$ and $L_{\alpha(dB)(2)}$ is less than 0.1 dB, R_1 may be taken as the final range value, and steps 12 through 14 may be omitted. If $L_{\alpha(dB)(1)}$ is less than 0.1 dB, R' may be taken as the final range value, and steps 9 through 14 may be omitted. (For radar frequencies up to 10,000 megahertz, correction of the atmospheric attenuation beyond the $L_{\alpha(dB)(2)}$ value would amount to less than 0.1 dB.)

(C) Fig. 31 — Detection range calculation worksheet completed for Mode 3 waveform; 0.5 P_d, 10^{-8} P_{fa} on a 1-m^2 target

search, is shaped to provide coverage at a constant altitude to an elevation angle of 70°. Shaping of the beam is accomplished by the row phase shifters used to stabilize and steer the beam in the elevation plane.

(C) Once a target is detected in the search mode, its range and azimuth are known. On a subsequent scan of the antenna past that azimuth, an elevation scan of the pencil beam pattern can be programmed to determine the height of the target. The range sweeps for these pulses need extend only slightly beyond the range at which the target was detected, thereby providing a significant saving of time. In addition, the elevation scan is terminated as soon as the target is seen. Since the antenna feed network provides monopulse signals in both the azimuth and elevation planes, an accurate determination can be made of the heights of targets that are more than one beamwidth above the horizon. Once a 3-D measurement of a target's position has been made, a 3-D track can be maintained on it by illuminating it with one or a few pulses on subsequent scans of the antenna; these pulses would be transmitted using the pencil-beam antenna pattern. Of course, time used to make the height measurements or update tracks is subtracted from the time available for search.

(C) Use of the mode is illustrated in Figs. 32 and 33. Events pictured in Fig. 32 are separated in time by at least one-half a rotation period (2 s). On the right side of the illustration, the beam pattern used for search is shown. On the left side, an elevation scan to determine the height of a target detected at 75 n.mi. on a prior antenna scan is depicted. Figure 33 shows a possible use of the pulses available during the rotation of the antenna through one azimuth beamwidth. Updates are performed on two targets in track, which are located within that azimuth sector, and the remainder of the time is devoted to search pulses transmitted in the fan-beam pattern.

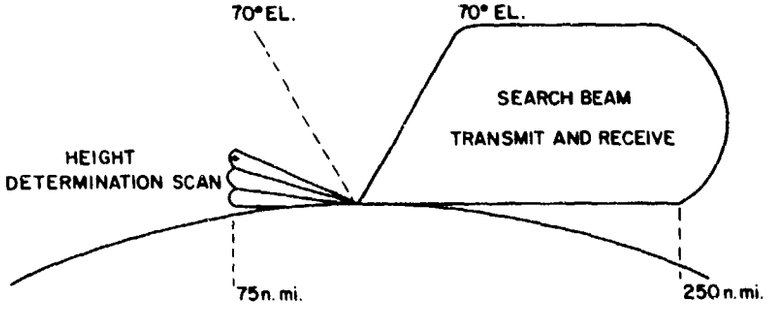

(C) Fig. 32 — Fan-beam search mode (Mode 4)

(C) If a center frequency azimuth beamwidth of 3.53° is assumed, with a 4-s data rate, there are 39.2 ms available during the rotation of the antenna through one azimuth beamwidth. With an instrumented range of 250 n.mi., it would be possible to transmit 11.2 pulses during that time. If the range sweep were limited to 125 n.mi., 22.4 pulses could be transmitted. Either range sweep should provide relatively good MTI performance, although

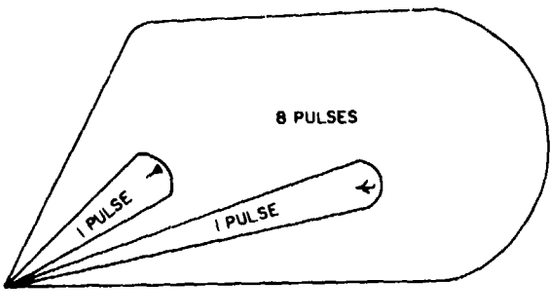

(C) Fig. 33 — Hypothetical utilization of energy available during antenna rotation through one azimuth beamwidth

the performance will be considerably better with the shorter range sweep, because of the greater number of pulses and higher PRF.

(C) A calculation showing the radar sensitivity of this mode against a 5-m^2 target is presented in Fig. 34. This calculation is made for an instrumented range of 250 n.mi., and assumes that two groups of MTI pulses are transmitted (6 pulses per group) and that the two outputs from the MTI processor are noncoherently integrated. The predicted detection range is 182 n.mi. It should be noted that this calculation does not purport to show the performance in a clutter environment (i.e., the improvement factor realized in signal-to-clutter (S/C) ratio), since that would be a function of the clutter model assumed and of the specific implementation of the MTI filter. If the improvement factor were sufficient to reduce the clutter residue to the noise level, the range calculated here would be the expected detection range. With an instrumented range of 125 n.mi., four MTI pulse groups could be processed and the sensitivity would be sufficient to detect a 1-m^2 Swerling Case 1 target at 119 n.mi.

Signal Processing

(C) Each signal processing unit shown in Fig. 23 performs the functions of MTI processing, pulse compression, and signal thresholding to maintain a constant false-alarm rate. A simplified block diagram of one of the receiver-processor units is shown in Fig. 35.

(C) MTI processing precedes pulse compression in order to reduce the dynamic range requirements in the pulse compression circuitry. Ten-bit A/D converters are used to digitize incoming signals. For Mode 1 operation, the lower MTI channel, with f' frequency input, is implemented only to 20 n.mi., whereas the upper channel is implemented to 125 n.mi. Each MTI channel may be bypassed for those modes or beam positions in which MTI processing is not desired. Signals from the f' channel are passed to the video integrator during the first 20 n.mi. of the range sweep. At that point, the position of the switch at the input to the video integrator is changed to accept inputs from the f channel for the remainder of the range sweep.

(C) Digital pulse compression techniques permit the accommodation of a variety of uncompressed pulse lengths, as required in the energy management program used in the elevation scan.

PULSE-RADAR RANGE-CALCULATION WORK SHEET

For use in conjunction with NRL Report 6930 (Dec. 1969). Based on Eq. (13), page 10, and associated auxiliary equations and curves as referenced below.

1. Compute the system input noise temperature T_s, following the outline in section A below.
2. Enter range factors known in other than decibel form in section B below, for reference.
3. Enter logarithmic and decibel values in section C below, positive values in the plus column and negative values in the minus column. For example, if $V_{0\,(dB)}$ as given by Figs. 4 through 9 is negative, then $-V_{0\,(dB)}$ is positive and goes in the plus column. For C_B, see Figs. 1 through 3. For definitions of the range factors, see Eq. (13).

Radar antenna height: h = ft. Target elevation angle: $\theta = 0.5°$. (See Fig. 13.)

A. Computation of T_s:

$T_s = T_a + T_r + L_r T_e$

(a) Compute T_a.
For $T_{tg} = T_{ta} = 290$ and $T_g = 36$ use Eq. (37a).
Read T_a' from Fig. 11.
$L_{a(dB)}$: 1.6 L_a: 1.445
$T_a = (0.876\,T_a' - 254)/L_a + 290$
T_a = 175°K

(b) Compute T_r using Eq. (40).
For $T_{tr} = 290$ use Table 1.
$L_{r(dB)}$: 1.6 T_r = 129 °K

(c) Compute T_e using Eq. (41) or using Table 1.
$F_{n(dB)}$: 4 T_e: 438 °K
L_r: 1.445 $L_r T_e$ = 633°K

Add. T_s = 937 °K

B. Range Factors		C. Decibel Values	Plus (+)	Minus (-)
$P_{t\,(kW)}$	25	10 log $P_{t\,(kW)}$	14.0	.
$\tau_{\mu sec}$	400	10 log $\tau_{\mu sec}$	26.0	.
G_t	1260	$G_{t(dB)}$	31.0	.
G_r	1260	$G_{r(dB)}$	31.0	.
$\sigma_{(sq\,m)}$	5	10 log σ	7.0	.
f_{MHz}	1125	-20 log f_{MHz}	.	61.0
T_a (°K)	937	-10 log T_a	.	29.7
V_0	2 pulses	$-V_{0\,(dB)}$	.	11.5
C_B	—	$-C_{B(dB)}$		—
L_t		$-L_{t(dB)}$		1.6
L_p		$-L_{p(dB)}$		1.6
L_x		$-L_{x(dB)}$		3.0
Range-equation constant (40 log 1.292)			4.45	
4. Obtain the column totals →			113.5	108.4
5. Enter the smaller total below the larger →			108.4	.
6. Subtract to obtain the net decibels (dB) →			+5.1	- .

7. In Table 2 find the range ratio corresponding to this net decibel (dB) value, taking its sign (±) into account. Multiply this ratio by 100. This is R_0 → 134
8. Multiply R_0 by the pattern-propagation factor F = 1.56 (see Eqs. (42) through (65) and Figs. 12 through 19):
$R_0 \times F = R'$ → 209
9. On the appropriate curve of Figs. 21 and 22 determine the atmospheric-absorption loss factor, $L_{a(dB)}$, corresponding to R'. This is $L_{a(dB)(1)}$. → 2.35
10. Find the range factor δ_1 corresponding to $-L_{a(dB)(1)}$ from the formula δ = antilog $(-L_{a(dB)}/40)$ or by using Table 2. → .8735
11. Multiply R' by δ_1. This is a first approximation of the range R_1. → 182
12. If R_1 differs appreciably from R', on the appropriate curve of Figs. 21 and 22, find the new value of $L_{a(dB)}$ corresponding to R_1. This is $L_{a(dB)(2)}$. →
13. Find the range-increase factor (Table 2) corresponding to the difference between $L_{a(dB)(1)}$ and $L_{a(dB)(2)}$. This is δ_2. →
14. Multiply R_1 by δ_2. This is the radar range in nautical miles, R. →

Note: If the difference between $L_{a(dB)(1)}$ and $L_{a(dB)(2)}$ is less than 0.1 dB, R_1 may be taken as the final range value, and steps 12 through 14 may be omitted. If $L_{a(dB)(1)}$ is less than 0.1 dB, R' may be taken as the final range value, and steps 9 through 14 may be omitted. (For radar frequencies up to 10,000 megahertz, correction of the atmospheric attenuation beyond the $L_{a(dB)(1)}$ value would amount to less than 0.1 dB.)

(C) Fig. 34 — Detection range calculation worksheet completed for Mode 4; 0.5 P_d, 10^{-8} P_{fa} on a 5-m^2 target

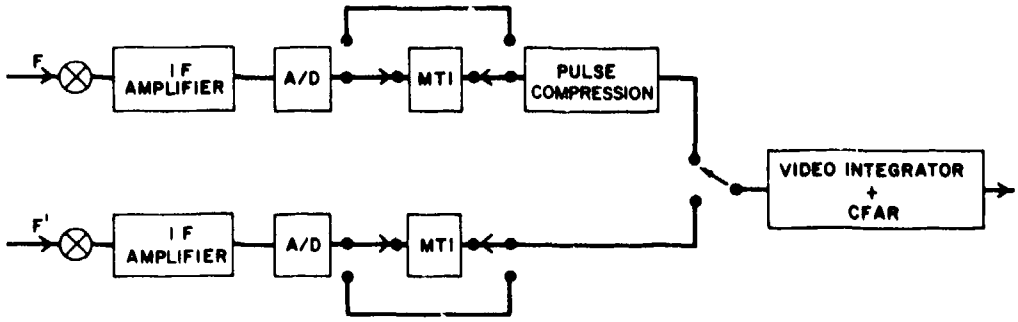

(C) Fig. 35 — Receiver-processor for 3-D radar

(U) After integration and thresholding, the sum, azimuth difference, and elevation difference signals are routed to the data processor.

Data Processing

(C) In the data-processor section of the radar, monopulse signals are processed in conjunction with beam-position commands and ship attitude information from the stable element to generate target position estimates. Data for each detection are compared with the positions of targets currently in the track file. If a target falls within a correlation cell of a target currently in the track file, it is treated as an update of that track. If a detection cannot be correlated with a current track, it is considered as a tentative new track. After a number of detections of a new target are made, a velocity vector is generated for it, and it is entered in the track file.

(C) The number of tracks that can be maintained is a function primarily of the capacity and speed of the computer and of the data processor, but it is also a function of the correlation cell size; this, in turn, is a function of the radar beamwidth and compressed pulse length and also depends on target speed and assumed maneuvering capabilities. The radar-data processor combination will have a track capacity of at least 250 targets.

(U) Output information from the data processor goes to displays and to various user stations such as command and control and weapon control centers.

SUMMARY

(C) Frequency agility over a wide band provides a number of performance benefits for shipboard air surveillance radars: (a) vulnerability to ECM is reduced, (b) multipath interference nulls are greatly reduced in depth and number, (c) MTI blind speeds are effectively eliminated, and (d) detectability of slowly fluctuating targets is improved. Concepts for both 2-D and 3-D radars are described in this report, each having a capability of pulse-to pulse frequency agility over approximately a 50% band. The 2-D radar is described in greater detail, since the effort to date has been concentrated on that system.

(C) In addition to the 50% agility bandwidth, features of the 2-D radar concept include an antenna stabilized against roll and pitch and a 4-s data rate. These two features should permit direct handover of a target from the 2-D radar to a weapon control radar, thereby eliminating the need for a 3-D surveillance radar on some ships. A sophisticated MTI system is employed to permit detection of small targets in rain or chaff at long ranges and to permit detection of targets at ranges where both land clutter and rain or chaff compete with the target return. The sophisticated MTI system, together with the absence of interference nulls and MTI blind speeds, should result in superior automatic detection and automatic tracking performance.

ACKNOWLEDGMENT

The basic concept for this radar was suggested by Dr. Merrill I. Skolnik. Several others, notably Dr. R. J. Adams, have contributed to the evolution of the approaches presented herein.

REFERENCE

1. L. V. Blake, "A Guide to Basic Pulse-Radar Maximum Range Calculation: Part 1, Equations, Definitions, and Aids to Calculations," NRL Report 6930, Dec. 23, 1969.

2. L. V. Blake, "Machine Plotting of Radio/Radar Vertical-Plane Coverage Diagrams," NRL Report 7098, Jun. 25, 1970.

3. A. W. Rihaczek, "A Systematic Approach to Blind-Speed Elimination," IEEE Trans. AES-9, No. 6, 940-947 (Nov. 1973).

4. J. K. Hsiao, and F. Kretschmer, Jr., "Design of a Staggered-PRF MTI Filter," NRL Report 7545, Jan. 30, 1973.

5. B. H. Cantrell, and G. V. Trunk, "Analysis of the Track Handoff Between the Search and Track Radars," NRL Report 7505, Dec. 29, 1972.

6. W. L. Thrift, "An Experimental Broadband L-Band Dipole (Project DUBSUR)," NRL Memorandum Report 2730 (Confidential Report, Unclassified Title), Feb. 1974.

7. Raytheon Tentative Product Specification, Electron Tube, Traveling Wave Amplifier, Type QKW1518SG, dated Apr. 10, 1973 and test data supplied to NRL by Raytheon on Apr. 3, 1973.

8. G. V. Trunk, "Comparison of Two Scanning Radar Detectors: The Moving Window and the Feedback Integrator," IEEE Trans. AES-7, No. 2, 395-398 (Mar. 1971).

9. F. E. Nathanson, *Radar Design Principles*, McGraw-Hill, New York, 1969.

10. J. K. Hsiao, "Performance Simulation of a Multiple-Stage MTI and Doppler Filter System," NRL Report 7829.

11. W. H. Perkins, General Electric Co., private communication, Feb. 1974.

12. R. D. Tompkins, editor, "SENRAD: An Advanced Surveillance Radar Concept," NRL Report 7713 (Secret Report, Unclassified Title), May 22, 1974.

13. J. K. Hsiao, and A. G. Cha, "On the Optimization of Clutter Rejection of a Nonrecursive Moving Target Indication Filter," NRL Report 7622, Nov. 12, 1973.

14. L. F. Fehlner, "Marcum's and Swerling's Data on Target Detection By a Pulsed Radar," Johns Hopkins University Applied Physics Laboratory Report TG 451, July 2, 1962.

(Page 48 Blank)

UNITED STATES GOVERNMENT

memorandum

5300-24
11 June 1998

DATE:

REPLY TO ATTN OF: Code 5301

SUBJECT: REQUEST TO DOWNGRADE NRL REPORT 7848

TO: Code 1221.1CR OK 6/29/98

1. It is requested that NRL Report 7848, "Shipboard Air Surveillance Radar Concepts: SENRAD I," dated 17 January 1975 be downgraded from its current classification of "Unclassified, Distribution Limited to U.S. Government Agencies Only," to "Unclassified, Approved for Public Release."

2. The information in this unclassified report no longer needs to have a restricted distribution since the technology described dates back to the 1970s, it has not and is not now being used by the U.S. Navy, and we no longer expect to apply this particular technology to future Navy radars or other U.S. military radars.

Edward E. Maine

EDWARD E. MAINE
Associate Superintendent
Radar Division

AD-C000 914

Completed
15 May 2000
R.W.

OPTIONAL FORM NO. 10
(REV. 1-80)
GSA FPMR (41 CFR) 101-11.6
5010-114